

1 **Biochemical analysis of coronavirus spike glycoprotein conformational intermediates**  
2 **during membrane fusion**

3

4 Miyuki Kawase<sup>a</sup>, Michiyo Kataoka<sup>b</sup>, Kazuya Shirato<sup>a</sup>, and Shutoku Matsuyama<sup>a\*</sup>

5

6 <sup>a</sup>Department of Virology III, National Institute of Infectious Diseases, Murayama Branch, 4-  
7 7-1 Gakuen, Musashi-murayama, Tokyo 208-0011, Japan

8 <sup>b</sup>Department of Pathology, National Institute of Infectious Diseases, Murayama Branch, 4-7-  
9 1 Gakuen, Musashi-murayama, Tokyo 208-0011, Japan

10

11 **Running title:** Coronavirus spike activation

12

13 \* Address correspondence to matuyama@nih.go.jp

14 Department of Virology III, National Institute of Infectious Diseases, Murayama Branch,  
15 4-7-1 Gakuen, Musashi-Murayama, Tokyo 208-0011, Japan

16 Tel: +81-42-561-0771 (ext. 3367); Fax: +81-42-567-5631

17

18 Abstract word count = 247

19 Main text word count = 8986

20

21 **Abstract**

22 A fusion protein expressed on the surface of enveloped viruses mediates fusion of the viral  
23 and cellular membranes to facilitate virus infection. Pre- and post-fusion structures of viral  
24 fusion proteins have been characterized, but conformational changes between them remain  
25 poorly understood. Here, we examined the intermediate conformation of the murine  
26 coronavirus fusion protein, called the spike protein, which must be cleaved by a cellular  
27 protease following receptor binding. Western blot analysis of protease digestion products  
28 revealed that two subunits (67 and 69 kDa) are produced from a single spike protein (180  
29 kDa). These two subunits were considered to be by-products derived from conformational  
30 changes and were useful for probing the intermediate conformation of the spike protein.  
31 Interaction with a heptad repeat (HR) peptide revealed that these subunits adopt packed and  
32 unpacked conformations, respectively, and two-dimensional electrophoresis revealed a  
33 trimeric assembly. Based on biochemical observations, we propose an asymmetric trimer  
34 model for the intermediate structure of the spike protein. Receptor binding induces the  
35 membrane-binding potential of the trimer, in which at least one HR motif forms a packed-  
36 hairpin structure, while membrane fusion subunits are covered by the receptor-binding  
37 subunit, thereby preventing the spike protein from forming the typical homotrimeric pre-  
38 hairpin structure predicted by the current model of class I viral fusion protein. Subsequent  
39 proteolysis induces simultaneous packing of the remaining unpacked HRs upon assembly of  
40 three HRs at the central axis to generate a six-helix bundle. Our model proposes a key  
41 mechanism for membrane fusion of enveloped viruses.

42

43 **Importance**

44 Recent studies using single-particle cryo-electron microscopy (cryoEM) revealed the  
45 mechanism underlying activation of viral fusion protein at the priming stage. However,

46 characterizing the subsequent triggering stage underpinning transition from pre- to post-  
47 fusion structures is difficult because single-particle cryoEM excludes unstable structures that  
48 appear as heterogeneous shapes. Therefore, population-based biochemical analysis is needed  
49 to capture features of unstable proteins. Here, we analyzed protease digestion products of a  
50 coronavirus fusion protein during activation; their sizes appear to be affected directly by the  
51 conformational state. We propose a model for the viral fusion protein in the intermediate  
52 state, which involves a compact structure and conformational changes that overcome steric  
53 hindrance within the three fusion protein subunits.

54

55 **Introduction**

56 Class I viral fusion proteins drive the fusion of viral and cellular membranes to facilitate  
57 insertion of the viral genome into the host cytoplasm (1). Structural analyses including cryo-  
58 electron microscopy (cryoEM) and X-ray crystallography revealed pre- and post-fusion  
59 structures, and biochemical analysis led to the proposal of a unified model for conformational  
60 changes of viral fusion proteins; receptor binding primes the formation of a membrane-  
61 embedded homotrimeric pre-hairpin structure that bridges viral and cellular membranes, then  
62 folds back on itself to form a hairpin structure, drawing the viral and cellular membranes into  
63 close proximity, resulting in lipid mixing (1–3). The post-fusion form consists of a central N-  
64 terminal trimeric  $\alpha$ -helical coiled-coil (trimer of heptad repeat 1, HR1) surrounded by three  
65 C-terminal helices (HR2), generating a six-helix bundle (6HB) (1–3).

66 The molecular rearrangements occurring at the early stages of the fusion process  
67 underpinning the receptor-binding step in the fusion protein of human immunodeficiency  
68 virus-1, influenza virus, and coronavirus were revealed by high-resolution cryoEM (4–13).  
69 However, the dynamic rearrangements underpinning the transition from pre- to post-fusion  
70 structures remain largely uncharacterized. During membrane fusion in influenza virus and  
71 herpes simplex virus, V- or Y-shaped density was observed in the intermediate state by  
72 cryoEM (14, 15), and in the retroviral Env trimer, an asymmetric intermediate appeared to  
73 emanate from a single protomer in cryo-electron tomography experiments (16). For the  
74 Moloney murine leukemia virus Env protein, the sequential release of the surface subunit  
75 from the transmembrane subunit induces the formation of an asymmetric trimer (17).  
76 Adoption of an asymmetric conformation presumably overcomes steric hindrance within the  
77 three fusion protein subunits.

78 The coronavirus spike (S) glycoprotein is a class I viral fusion protein constructed of  
79 S1 and S2 subunits. The N-terminal S1 subunit is responsible for receptor binding, and the C-

80 terminal membrane-anchored S2 subunit is important for virus-cell membrane fusion. Some  
81 coronaviruses, such as severe acute respiratory syndrome coronavirus (SARS-CoV), Middle  
82 East respiratory syndrome coronavirus (MERS-CoV), and mouse hepatitis virus type 2  
83 (MHV-2), possess uncleaved 180 kDa S proteins. These viruses utilize cell surface or  
84 endosomal proteases (such as TMPRSS2, HAT, trypsin, elastase, or cathepsin L) to cleave S  
85 proteins during cell entry (2, 18–31). It remains controversial whether MERS-CoV S protein  
86 is processed by the cellular protease furin after internalization via endocytosis (32) because  
87 this finding was not supported by a recent study (33).

88         Our previous study showed that the S protein of MHV-2 requires a two-step  
89 conformational change process (26). The first step takes place after binding to a soluble form  
90 of the MHV receptor (CEACAM1a), upon which the metastable form of S protein is  
91 converted to a stable trimer possessing liposome-binding activity. The subsequent step is  
92 driven by protease digestion. From a single 180 kDa S protein, trypsin produces a 90 kDa  
93 subunit in the absence of receptor, but a 66 kDa subunit in the presence of receptor, and this  
94 66 kDa species is thought to involve the formation of a 6HB structure (detected as a  
95 proteinase K-resistant 53 kDa subunit) (26). A similar result of the protease digestion pattern  
96 was also reported in SARS-CoV and MERS-CoV S proteins (4, 20). Therefore, the sizes of  
97 protease digestion products are thought to be directly affected by the conformational state of  
98 the coronavirus S protein. Studying the MHV-2 S protein could illuminate the conformational  
99 changes occurring in each step, and may provide novel insight into viral class I fusion  
100 protein.

101

## 102 **Materials and methods**

### 103 **Virus, cells, soluble receptor, and HR2-mimicking peptide**

104 MHV-2 was propagated in DBT cells cultured in Dulbecco's modified Eagle's medium  
105 (DMEM) containing 10% tryptose phosphate broth (BD Difco, USA) (34). Viruses were  
106 collected at 21 h post-infection and stored at -80°C. The soluble form of the MHV receptor  
107 (CEACAM1a) was produced using recombinant baculovirus and purified as previously  
108 described (35). HR2-mimicking peptide  
109 (DLSLDFEKLNVTLDDLTYEMNRIQDAIKKLNESYINLKE) was provided by B. J. Bosch  
110 (36) and dissolved in water at a concentration of 500 µM.

111

#### 112 **Proteases and protease inhibitors**

113 Trypsin (T8802; Sigma, USA), proteinase K (166-21051; Wako, Japan), endoproteinase arg-  
114 C (P6056; Sigma), and endoproteinase lys-C (P3428; Sigma) were employed after being  
115 dissolved in phosphate-buffered saline (PBS; pH 7.4). Inhibitors camostat (3193; Tocris  
116 Bioscience, UK), Pefabloc SC (11429868001; Roche, Switzerland), and E64d (330005;  
117 Calbiochem, USA) were dissolved in dimethyl sulfoxide (DMSO). Soybean trypsin inhibitor  
118 (STI; T-9128; Sigma) was dissolved in PBS.

119

#### 120 **Liposomes**

121 Lipids 1-phosphatidylcholine (PC; egg; Avanti-Polar Lipids, USA), 1-  
122 phosphatidylethanolamine (PE; egg; Avanti-Polar Lipids), sphingomyelin (Sph; brain;  
123 Avanti-Polar Lipids), and cholesterol (Chol; Sigma) were mixed in a 1:1:1:1.5 molar  
124 PC:PE:Sph:Chol ratio, dried under N<sub>2</sub> gas in a glass tube, and lyophilized overnight. After  
125 addition of 1 ml of PBS (pH 7.2), the lipid suspension was vortexed and extruded 25 times  
126 through a 0.4 µm Nucleopore filter (GE Water & Process Technologies, USA) using an  
127 Avanti Mini-Extruder. Liposomes were stored at 4°C and used within 1 week.

128

129 **Activation of MHV-2 spike (S) protein and western blot analysis**

130 **Standard reaction.** To evaluate conformational changes in the S protein occurring in the first  
131 step, a 10  $\mu$ l solution of MHV-2 ( $10^7$  pfu/100  $\mu$ l) was mixed with 1.1  $\mu$ l of soluble receptor  
132 (10  $\mu$ M) and warmed at 37°C for 30 min. For conformational changes in the second step, 1.2  
133  $\mu$ l of trypsin (100  $\mu$ g/ml) was added and incubated at 37°C for 30 min. A 1/4 volume of  
134 sample buffer comprising 30% glycerol, 250 mM TRIS pH 6.8, 2.5% sodium dodecyl sulfate  
135 (SDS), a small amount of Bromophenol Blue, 100 mM dithiothreitol (DTT), and 1 mM  
136 Pefabloc SC was added to the reaction and boiled at 100°C for 5 min. Samples were  
137 separated by sodium dodecyl sulfate polyacrylamide gel electrophoresis (SDS-PAGE) on  
138 3–10% gradient or 7.5% gel (e-PAGEL; ATTO, Japan), transferred to a polyvinylidene  
139 difluoride (PVDF) membrane (Immobilon-P; Millipore, USA), and soaked in ImmunoBlock  
140 (CTKN001; DS Pharma Biomedical, Japan) for 5 min. Western blot analysis was carried out  
141 using anti-S2 antibodies, a mouse monoclonal antibody recognizing the 10G epitope (MAb-  
142 10G), and rabbit anti-peptide antibodies recognizing the S2a region, the very highly  
143 conserved region (VHCR), and cytoplasmic tail (CT) epitopes (anti-S2a, anti-VHCR, and  
144 anti-CT, respectively), followed by horseradish peroxidase-conjugated anti-mouse (32430;  
145 Thermo, USA) or anti-rabbit (sc-2054; Santa Cruz Biotech, USA) IgG. Immunoreactive  
146 bands were visualized with an enhanced chemiluminescence kit (ECL; RPN2232; GE  
147 Healthcare, USA) and a LAS-3000 instrument (Fuji, Japan). All experiments were repeated at  
148 least twice.

149 **Reactions in the presence of liposomes.** A 6  $\mu$ l sample of liposomes was added, and the  
150 volume of receptor and trypsin was raised to achieve the target concentrations. Standard  
151 reactions were then carried out as described above.

152 **Timing of heptad repeat (HR) packing.** To stop the reaction at the indicated time points,  
153 reactions were quickly frozen in dry ice/methanol, and 1.4  $\mu$ l of HR2-mimicking peptide (500

154  $\mu\text{M}$ ) was added. Samples were further incubated at  $37^\circ\text{C}$  for 20 min to facilitate the formation  
155 of 67 and 69 kDa fragments.

156 **Generation of the proteinase K-resistant 53 kDa fragment.** After assessing conformational  
157 changes of the S protein as described above, reaction mixtures were chilled on ice for 5 min  
158 and 1.5  $\mu\text{l}$  of proteinase K (10 mg/ml) was added and incubated on ice for 30 min.

159 **Deglycosylation of the S2 subunit.** After assessing conformational changes of the S protein  
160 as described above, deglycosylation was carried out using Protein Deglycosylation Mix  
161 (P6039S; NEB, UK) according to the manufacturer's instructions.

162 **SDS-PAGE of unboiled samples (native PAGE).** After assessing conformational changes of  
163 the S protein as described above, sample buffer excluding DTT was added and unboiled  
164 mixtures were separated by SDS-PAGE (3–10% gradient or 7.5% gel; e-PAGEL).

165 **Protein denaturation on PVDF membranes.** After SDS-PAGE of unboiled samples and  
166 electro transfer to a PVDF membrane, initial detection of native S protein was performed by  
167 western blot analysis. The membrane was then soaked in stripping buffer (46428;  
168 ThermoFisher, USA) at room temperature for 5 min to denature the S protein, rinsed 10 times  
169 with rinse buffer (20845; Millipore), blocked with ImmunoBlock, and re-probed with anti-S2  
170 antibody.

171 **Two-dimensional SDS-PAGE.** S protein was treated with receptor and trypsin as described  
172 above, mixed with sample buffer containing molecular size markers (1610373; BioRad,  
173 USA) without DTT, and separated by SDS-PAGE using a 3–10% gradient gel (first gel).  
174 After electrophoresis, the gel was wrapped in a heat-seal bag, soaked in sample buffer (0.5%  
175 SDS), boiled at  $105^\circ\text{C}$  for 5 min in an autoclave, sliced along the protein markers, placed  
176 onto a 7.5% gel (second gel), and subjected to electrophoresis and western blot analysis.

177

178 **Generating trypsin-treated MHV-2 harboring cleaved S protein**

179 A solution of MHV-2 (500  $\mu$ l;  $10^7$  pfu/100  $\mu$ l) was mixed with 5  $\mu$ l of trypsin (100  $\mu$ g/ml) or  
180 PBS (for uncleaved control) and incubated at 37°C for 1 h. Next, 5  $\mu$ l of STI (10 mg/ml in  
181 PBS) and 5  $\mu$ l of camostat (1 mM in PBS) were added and incubated at room temperature for  
182 10 min to inactivate trypsin. About 500  $\mu$ l of virus solution was applied to a 2 ml bed volume  
183 of Sephadex G-75 (17005101; GE Healthcare) equilibrated with PBS (column size, 10 ml)  
184 (7311550; BioRad, USA). PBS (1.4 ml) was loaded onto the column, and eluent (200  $\mu$ l  
185 fractions) was collected. Western blot analysis was carried out using MAb-10G to identify  
186 fractions containing MHV-2. Fractions 3 and 4 were used for the experiments shown in  
187 Figure 2.

188

#### 189 **Virus cell entry assay**

190 DBT cells in a collagen-coated 96-well culture plate (4860-010; Iwaki, Japan) were treated  
191 with DMEM containing 10  $\mu$ M E64d cathepsin inhibitor at 37°C for 30 min to block the  
192 endosomal virus entry pathway. Approximately  $10^5$  pfu of virus was used to infect  $10^5$  cells  
193 on ice. After a 30 min adsorption on ice, virus was removed and cells were treated with  
194 various concentrations of trypsin. After a 30 min incubation, viral entry was stopped by  
195 adding DMEM containing 10  $\mu$ M camostat and 10  $\mu$ M E64d, and incubated at 37°C for 5 h.  
196 Cellular RNA was isolated from cells with the addition of 200  $\mu$ l of Isogen (311-02501;  
197 Nippon Gene, Japan). Real-time PCR was performed to estimate the amount of newly  
198 synthesized viral mRNA<sub>7</sub> as described below.

199

#### 200 **Quantitative estimation of viral mRNA by real-time PCR**

201 Real-time reverse transcription PCR was performed to estimate the amount of MHV-2  
202 mRNA<sub>7</sub> as described previously. The target sequence was the MHV-2 N gene. Hybridization  
203 probes labeled with fluorescent dye, 5'-GCTCCTCTGGAAACCGCGCTGGTAATGG-3'

204 (3'-labeled with fluorescein isothiocyanate) and 5'-  
205 ATCCTCAAGAAGACCACTTGGGCTGACCAAACC-3' (5'-labeled with LCR640),  
206 were used to detect the amplified fragments. To amplify viral mRNA7, oligonucleotides 5'-  
207 GTACGTACCCTTTCTACTC-3' (MHV-2 leader) and 5'-CAAGAGTAATGGGGAACCA-  
208 3' (MHV-2 mRNA7 reverse) were employed. PCR analysis involved reverse transcription at  
209 61°C for 20 min, followed by PCR with an initial denaturation at 95°C for 30 s, followed by  
210 40 cycles at 95°C for 5 s, 55°C for 15 s, and 72°C for 13 s. Reactions were performed using a  
211 LightCycler Nano instrument (Roche). The amount of virus in cells was calculated from the  
212 calibration curve.

213

#### 214 **Electron microscopy**

215 A 6 µl aliquot of ultraviolet-irradiated virus was absorbed onto glow-discharged 300-mesh  
216 heavy-duty carbon-coated Cu grids (Veco grids; Nisshin EM, Tokyo, Japan) for 2 min, and  
217 the excess was blotted onto filter paper (Whatman; GE Healthcare, Piscataway, NJ, USA).  
218 Grids were then washed twice with Milli-Q water and negatively stained with 2%  
219 phosphotungstic acid. Data were collected using an HT7700 transmission electron  
220 microscope (Hitachi, Tokyo, Japan) operating at 100 kV electrons and magnification of  
221 30,000×.

222

#### 223 **Statistical analysis**

224 Two-tailed Student's t-tests were used to analyze statistical significance. A *p*-value <0.05  
225 was considered statistically significant. n.s. = not significant, \* = significant ( $p \leq 0.05$ ), \*\* =  
226 highly significant ( $p \leq 0.01$ ), \*\*\* = very highly significant ( $p \leq 0.001$ ). Error bars indicate  
227 standard deviation (SD).

228

229 **Results**

230 **Trypsin digestion generates three different sizes (90, 69, and 67 kDa) of S2 subunit**

231 A schematic diagram of the MHV-2 S protein and the binding sites of antibodies employed in  
232 this study is shown in Figure 1A. Three anti-synthetic peptide antibodies, anti-S2a, anti-  
233 VHCR, and anti-CT, and a monoclonal antibody (MAb-10G) were used to detect the S2  
234 subunits via western blot analysis. To probe conformational changes of the MHV-2 S protein,  
235 an authentic virus rather than recombinant S protein was employed. Virus at  $10^6$  plaque-  
236 forming units (pfu) in 10  $\mu$ l of culture medium was treated with the soluble form of the MHV  
237 receptor (1  $\mu$ M) at 37°C for 30 min, and 10  $\mu$ g/ml trypsin was added and incubated for 30  
238 min. The main difference between previous (26) and present experiments is the concentration  
239 of trypsin (10  $\mu$ g/ml trypsin was used instead of 1  $\mu$ g/ml trypsin).

240 As reported previously (26), trypsin-mediated cleavage of the 180 kDa S protein (Fig.  
241 1B, 10G and CT, lane 1) generated a species of 90 kDa (Fig. 1B, 10G and CT, lane 2) in the  
242 absence of receptor. However, two different S2 subunit fragments (67 and 69 kDa) were  
243 observed following trypsin-mediated cleavage in the presence of receptor (Fig. 1B, 10G and  
244 CT, lane 4). The 67 kDa subunit was observed for the first time when a higher concentration  
245 of trypsin (10  $\mu$ g/ml) was used in the present study. The sizes of these S protein subunits are  
246 revised from the previous study; the 200 kDa full-length S protein was revised to 180 kDa,  
247 the 80 kDa S2 subunit was revised to 90 kDa, and the 66 kDa S2 subunit was revised to 69  
248 kDa (26).

249 The appearance of the 90, 67, 69, and 53 kDa species was assessed at different trypsin  
250 concentrations. The 90 and 69 kDa species were detected following treatment with 0.25 or  
251 0.5  $\mu$ g/ml trypsin (Fig. 1C). In addition, a 67 kDa S2 subunit was observed when the  
252 concentration of trypsin was higher ( $\geq 1$   $\mu$ g/ml; Fig. 1C). Interestingly, both 67 and 69 kDa  
253 subunits were observed, even at the highest concentration of trypsin (128  $\mu$ g/ml), which is

254 ~100-fold higher than needed to induce conformational changes of S protein according to a  
255 previous report (26), suggesting that a heterogeneous mix of S2 subunits (67 and 69 kDa) was  
256 stably produced from a single (180 kDa) S protein species. Treatment with 1 mg/ml  
257 proteinase K was carried out to probe the post-fusion conformation that is thought to involve  
258 the formation of a 6HB structure (26). As shown in Figure 1C, a proteinase K-resistant 53  
259 kDa band was observed when the concentration of trypsin was  $\geq 0.125$   $\mu\text{g/ml}$  (lane 6).

260

### 261 **Quantification of virus cell entry triggered by trypsin**

262 The trypsin concentration required to induce virus cell entry was assessed. After virus  
263 adsorption for 30 min on ice, cells were treated with various concentrations of trypsin at 37°C  
264 for 30 min, and trypsin was then inactivated by addition of the serine protease inhibitor  
265 camostat mesylate. After a 5 h incubation at 37°C, cellular RNA was isolated and real-time  
266 PCR was performed to quantify viral subgenomic mRNA<sup>7</sup>. The concentration of trypsin  
267 required to induce viral cell entry was  $\geq 0.25$   $\mu\text{g/ml}$  (Fig. 1D), which corresponds  
268 approximately with the appearance of the 69 and 53 kDa fragments (Fig. 1C), but not the 67  
269 kDa fragment.

270

### 271 **Comparison of uncleaved and pre-cleaved S proteins**

272 As reported previously, the MHV-2f variant of MHV-2 harbors an amino acid substitution at  
273 the S1/S2 cleavage site that is cleaved by furin during biogenesis; this variant is sufficient to  
274 induce the cell-cell fusion without supplemental trypsin in the culture medium (29). To  
275 clarify whether cleavage at the S1/S2 site is sufficient for S protein priming prior to induction  
276 of conformational changes, we compared trypsin-treated MHV-2 and MHV-2f with MHV-2.  
277 To generate trypsin-treated MHV-2, the MHV-2 was exposed to 1  $\mu\text{g/ml}$  trypsin (or PBS for  
278 the uncleaved virus control) for 1 h, followed by addition of trypsin inhibitors (both STI and

279 camostat). Next, the viruses were purified using a Sephadex G-75 column. Figure 2A shows  
280 that, as reported previously (29), half of the S protein of MHV-2f was cleaved (lane 9)  
281 whereas almost all of the S protein expressed by the trypsin-treated virus was cleaved (lane 5)  
282 (compare with PBS-treated MHV-2 S protein (lane 1)). The trypsin-treated virus was able to  
283 enter cells as efficiently as the PBS-treated virus (Fig. 2B). Next, the viruses were exposed to  
284 both receptor and trypsin to induce conformational changes. A higher concentration of  
285 trypsin (50  $\mu\text{g/ml}$ ) was needed to cleave the S protein, presumably due to residual trypsin  
286 inhibitors. Although background levels of the 67 and 69 kDa products were observed in the  
287 absence of receptor (lane 6) (presumably due to the use of pre-incubated viruses), clear  
288 production of a 67 kDa fragment was observed in the presence of receptor and trypsin (lane  
289 8). Interestingly, induction of the proteinase K-resistant 53 kDa band from the trypsin-treated  
290 virus was observed in the presence of receptor, even in the absence of trypsin (lane 7); by  
291 contrast, the other two viruses (PBS-treated MHV-2 and MHV-2f) required both receptor and  
292 trypsin. This implies that the two types of cleaved S protein have different conformations: the  
293 pre-cleaved S protein (cleaved by furin during biogenesis) needs additional cleavage after the  
294 receptor-binding step, whereas the trypsin-treated S protein (cleaved on virus particle) needs  
295 only receptor binding to trigger the conformational changes. Cleavage at the S2' site (to  
296 generate the 69 kDa species) may trigger conformational changes, as reported previously (20,  
297 30); however, cleavage at either the S1/S2 site or the S2' site is presumably enough to  
298 activate the MHV-2 S protein. The 67 and 69 kDa species can be considered by-products of  
299 the S protein following conformational changes; therefore, these products were examined to  
300 probe the intermediate conformation(s) of the S protein.

301

### 302 **Characterization of a 67 kDa S2 subunit**

303 As identified in previous studies using MHV and SARS-CoV, the 90 and 69 kDa subunits are  
304 derived from cleavage at the S1/S2 site (R756) and the S2' site (R907) (11, 19, 27, 28, 30,  
305 31). To identify the trypsin cleavage site that produces the 67 kDa fragment, we attempted to  
306 gain indirect evidence because the 67 kDa subunit has not been successfully purified from the  
307 virus particle for amino-terminal sequencing. Both the 67 and 69 kDa subunits were detected  
308 by MAb-10G and anti-CT, but not by anti-S2a, even following increased exposure of blots,  
309 and only the 69 kDa subunit was detected by anti-VHCR (Fig. 1B). These results indicate  
310 that the 69 kDa subunit is a product of cleavage between S2a and VHCR epitopes at the S2'  
311 site, as previously reported (11, 30), whereas the 67 kDa subunit is the result of cleavage at  
312 the C-terminal side of the VHCR epitope. Using endoproteinases arg-C and lys-C to identify  
313 the specific arginine or lysine residue of the cleavage site, the 67 kDa subunit was found to be  
314 cleaved at a lysine residue (Fig. 3A).

315 Next, deglycosylation of the S protein subunit was carried out using a commercial  
316 deglycosylation mix containing five enzymes that can completely remove *N*- and *O*-linked  
317 glycans from almost all glycoproteins except some plant and insect glycoproteins. The 90, 69,  
318 and 67 kDa bands were shifted to 65, 47, and 43 kDa, respectively, following treatment with  
319 0.32 or 32  $\mu\text{g/ml}$  trypsin (Fig. 3B). The 4 kDa size difference between 43 and 47 kDa  
320 deglycosylated bands indicates that the 67 kDa subunit is cleaved at K951 because the  
321 calculated molecular weight of the peptide fragment between S2' (R907) and K951 is 4.8  
322 kDa, whereas cleavage at the neighboring lysine K917 would yield a 1.3 kDa size difference,  
323 and cleavage at K1008 would afford a 10.6 kDa size difference. The K951 cleavage site was  
324 therefore designated postS2'. Notably, the postS2' cleavage site is in the 48th  $\beta$ -strand ( $\beta$ 48),  
325 which forms an anti-parallel  $\beta$ -sheet with  $\beta$ 47 in the pre-fusion form but not in the post-fusion  
326 form of the S protein (10, 11). Cleavage at postS2' is unlikely to contribute to S protein  
327 triggering because it is located at the C-terminal side of the fusion peptide (FP; Fig. 4A and

328 4B), and the appearance of the 67 kDa species does not correspond to the formation of the  
329 post-fusion structure (53 kDa) or virus entry (Fig. 1C and 1D), as described above.

330 Additional experiments were carried out to characterize the 67 kDa subunit. The  
331 receptor concentration was found to affect the total amount of 67 and 69 kDa species, but not  
332 the relative ratio between them (Fig. 3C), implying that two different cleavable features of the  
333 S2 subunit were induced in the receptor-binding step. Furthermore, inclusion of dithiothreitol  
334 (DTT) at concentrations  $\geq 1$  mM in the sample buffer shifted the 67 kDa band to a greater  
335 extent than the 69 and 90 kDa bands during SDS-PAGE (Fig. 3D). Two cysteine residues at  
336 positions 1169 and 1214 (Fig. 4A and 4B), between the HR1 and HR2 motifs (in the  
337 connector region), were predicted to affect the conformation of the 67 kDa subunit.  
338 Meanwhile, cysteine residues 932 and 943, located upstream of HR1, and residues 1119 and  
339 1130 within the invariant motifs may affect the smaller shift observed for the 69 and 90 kDa  
340 bands. The connector region, including the disulfide bond, presumably contributes to folding  
341 of the 67 kDa subunit, but not to that of the 69 and 90 kDa subunits.

342

#### 343 **Two different sizes of S2 subunit are present in the trimer**

344 We next turned our attention to how two different sizes of S2 subunit (67 and 69 kDa) could  
345 be produced by trypsin digestion of a single 180 kDa S protein species, even though a single  
346 sized (90 kDa) species is produced in the absence of receptor. We hypothesized that the S  
347 protein forms a heterogeneous trimer in the presence of receptor, so that each S protein in a  
348 trimer exposes a different cleavage site. In the first native SDS-PAGE step (gels were boiled  
349 before blotting so that the trimer could be detected by the antibody, as described in the  
350 methods), several different sizes of trimer were detected (Fig. 5A, lanes 2 and 3). In the  
351 second denaturing SDS-PAGE step, these trimer bands were separated into monomer bands  
352 (Fig. 5A, lanes 5 and 6). To examine the components of the trimer, we performed two-

353 dimensional electrophoresis. Following treatment with 10  $\mu\text{g/ml}$  trypsin, both the 67 and 69  
354 kDa bands, or the single 67 kDa band, were separated from three species of trimer at around  
355 140 kDa (Fig. 5B and 5C b), whereas only the 69 kDa band was detected following treatment  
356 with 0.32  $\mu\text{g/ml}$  trypsin (Fig. 5C a). These results suggest that a subset of S2 subunits can  
357 form a heterogeneous trimer comprising the 69 and 67 kDa species at a ratio of 3:0, 2:1, 1:2,  
358 or 0:3.

359

### 360 **Exposed or buried epitope configurations in the S protein globule**

361 Further characterization of S2 subunits was performed to investigate exposed and buried  
362 configurations of epitopes, and the results are shown in Figure 6A and 6B. MHV-2 was  
363 treated with receptor and trypsin to induce conformational changes as described above. S  
364 protein detection was performed using four anti-S2 antibodies recognizing linear epitopes.  
365 Following soaking in stripping buffer to denature the S protein on the polyvinylidene  
366 difluoride (PVDF) membrane, detection was then repeated with the same antibodies. When  
367 antibodies against the VHCR and CT epitopes were used, all bands detected in denatured  
368 blots (Fig. 6B) were the same as those observed in native blots (Fig. 6A), indicating that these  
369 epitopes are exposed on the S protein in both the native and denatured states. In the post-  
370 fusion form of the S protein treated with receptor and trypsin, doublet bands at 140 kDa were  
371 observed using anti-CT antibody (Fig. 6A, CT, lane 4), while lower bands were not observed  
372 with the anti-VHCR antibody (Fig. 6A, VHCR, lane 4). This observation correlates with the  
373 appearance of 67 and 69 kDa bands in SDS-PAGE (Fig. 1B, CT and VHCR, lane 4),  
374 suggesting that the upper band of 140 kDa species is composed of 67 and 69 kDa subunits,  
375 whereas the lower band comprises three 67 kDa subunits. This is consistent with the results in  
376 Figure 5C b showing that the 67 and 69 kDa bands were separated from 140 kDa trimer  
377 bands.

378 Using anti-S2a antibody recognizing a linear epitope (Fig. 1B, S2a) (37), a 500 kDa  
379 band corresponding to a trimeric assembly was observed only after the receptor-binding step  
380 in native blots (Fig. 6A, S2a, lane 3), as observed in a previous study (26), but this was barely  
381 detectable in denatured blots (Fig. 6B, S2a, lane 3). We do not currently have an explanation  
382 for exposure of the S2a epitope, but this hydrophobic epitope is buried in the globule in the  
383 pre-fusion state (10) and is presumably exposed only in the native trimer after the receptor-  
384 binding step, before disappearing following cleavage by trypsin. When antibody recognizing  
385 the 10G epitope was used, monomeric S2 subunit species were detected in the native blot  
386 (Fig. 6A, 10G, lanes 3 and 4), but trimeric species were not observed, although they were  
387 detectable in the denatured blot (Fig. 6B, 10G, lanes 3 and 4). This indicates that the 10G  
388 epitope adopts a buried configuration in the trimer of pre- and post-fusion forms. These  
389 observations provided clues that were used to predict the intermediate structure of the S2  
390 subunit.

391

### 392 **The timing of S protein cleavage**

393 We next analyzed the timing of the appearance of 67, 69, and 53 kDa fragments during  
394 conformational changes of the S protein. To stop the reaction after different incubation times  
395 at 37°C, reaction tubes were quickly frozen in dry ice/methanol, and immediately boiled in  
396 sample buffer containing the trypsin inhibitor. As shown in Figure 7A, trypsin treatment on  
397 ice for 5 min following receptor treatment was sufficient to generate the 69 kDa but not the  
398 proteinase K-resistant 53 kDa species (lane 2). The 53 kDa band was induced after a 1 min  
399 incubation at 37°C (lane 3), and the 67 kDa band appeared and became prominent over 4 min  
400 (lane 5), indicating that the conformational changes that induce the 6HB structure are  
401 complete at 1 min after treatment with trypsin. In preliminary EM experiments (described  
402 below), conformational changes of the S protein were probed in the presence of liposomes.

403 The appearance of S2 fragments (90, 69, and 67 kDa) and the timing of cleavage coinciding  
404 with their appearance were the same in the absence and presence of liposomes (Fig. 7B and  
405 7C).

406

#### 407 **Unpacked (accessible) and packed (occluded) HR conformations**

408 To characterize the conformational states of 67 and 69 kDa subunits after the receptor-  
409 binding step, HR2-mimicking peptide was employed. This 39 amino acid peptide derived  
410 from the HR2 region of the S2 subunit is water-soluble and interferes with packing of the  
411 HR1/HR2 motif, thereby inhibiting virus infection (36). MHV-2 pre-treated with soluble  
412 receptor was treated with HR2-mimicking peptide (50  $\mu$ M) and various concentrations of  
413 trypsin. The 69 kDa but not the 67 kDa subunit disappeared following treatment with HR2-  
414 mimicking peptide, and the 55 kDa degradation product appeared after incubation in the  
415 presence of 8  $\mu$ g/ml trypsin (Fig. 8A, lane 13). Presumably, protease-cleavable sites in the S2  
416 subunit are vulnerable to scission by trypsin when the HR2-mimicking peptide is present due  
417 to the restriction of helical bundle formation by the HR motif; hence the cleavage pattern was  
418 altered. This also indicates that the HR1/HR2 motif in the 67 kDa fragment forms a post-  
419 fusion species in which the HR1 motif is occluded after the receptor-binding step.

420 Interestingly, HR2-mimicking peptide completely inhibited production of the  
421 proteinase K-resistant 53 kDa fragment (Fig. 8C, lanes 11 and 13), even in the presence of  
422 the packed 67 kDa species (Fig. 8A, lanes 11 and 13), suggesting that HR2-mimicking  
423 peptide interferes with 6HB formation. The trimer in the receptor-binding step is presumably  
424 constructed from both packed and unpacked HR1/HR2 motifs, and HR2-mimicking peptide  
425 interacts with an unpacked motif, and thereby interferes with 6HB formation. In the presence  
426 of 0.5–2  $\mu$ g/ml trypsin, HR2-mimicking peptide did not appear to affect degradation of the 69  
427 kDa fragment due to the low concentration of trypsin (Fig. 8A, lanes 5–10). In addition,

428 trypsin degradation products in the presence of HR2-mimicking peptide were detected by  
429 MAb-10G antibody (Fig. 8A, lanes 13, 15, and 17) but not by anti-CT antibody (Fig. 8B,  
430 lanes 13, 15, and 17), indicating that the 10G epitope region is folded and consequently  
431 avoids cleavage by trypsin, whereas the C-terminal side of the 10G epitope including the  
432 HR2 region (residues 1253–1302, Fig. 4A) is presumably unfolded and therefore degraded by  
433 trypsin. Although the mechanism remains unknown, HR2-mimicking peptide enhanced the  
434 production of the 69 kDa subunit following treatment with 0.25  $\mu\text{g/ml}$  trypsin (Fig. 8B, lane  
435 3).

436 Next, the concentration dependence of HR2-mimicking peptide was assessed. In the  
437 presence of  $\geq 0.5 \mu\text{M}$  HR2-mimicking peptide, the 69 and 53 kDa bands disappeared (Fig. 8D  
438 and 8E, lanes 5–7), and the 55 kDa degradation products appeared (Fig. 8D, lanes 5–7). Pre-  
439 treatment of HR2-mimicking peptide with 10  $\mu\text{g/ml}$  trypsin did not affect the ability to cause  
440 the disappearance of the 69 and 53 kDa fragments (Fig. 8D and 8E, lanes 11–13), indicating  
441 that trypsin does not directly affect HR2-mimicking peptide. To determine whether the HR2-  
442 peptide actually blocks MHV-2 infection, real-time PCR-based virus entry assays were  
443 performed, as previously reported for SARS-CoV in which HR2-mimicking peptide blocks  
444 trypsin-mediated direct viral entry from the cell surface (38). In the presence of  $\geq 0.5 \mu\text{M}$   
445 HR2-mimicking peptide, virus entry was clearly blocked (Fig. 8F).

446

#### 447 **The timing of HR packing**

448 Next, the timing of HR1/HR2 motif packing in the S protein was analyzed. HR2-mimicking  
449 peptide was added to the S protein conformational change reaction at the indicated time  
450 points after stopping the reaction using dry ice/methanol, and mixtures were re-incubated at  
451 37°C for 20 min to facilitate production of the 67 and 69 kDa fragments (re-incubation is  
452 required to visualize bands that reflect the structure present upon HR2-mimicking peptide

453 addition). At each HR2-mimicking peptide addition time point, if the HR1/HR2 motif forms  
454 an unpacked structure, the HR2-mimicking peptide would be expected to bind to HR1 and  
455 trypsin would degrade the 69 kDa to produce the 55 kDa lacking the CT epitope as described  
456 above (Fig. 8A and 8B). As shown in Figure 8G (lane 2), the 67 kDa subunit appeared, the 69  
457 kDa subunit disappeared, and the 55 kDa degradation product appeared following treatment  
458 with HR2-mimicking peptide after the receptor-binding step, suggesting that both packed and  
459 unpacked HR1/HR2 motifs simultaneously occur in the reaction. After a 1 min incubation at  
460 37°C, undegraded 69 kDa subunit, which does not interact with HR2-mimicking peptide, was  
461 observed (Fig. 8G, lane 3), suggesting that both the 67 and 69 kDa fragments form a packed  
462 structure at this time point.

463

#### 464 **Assembly of three S2 subunits at the center of the S protein trimer**

465 As shown in Figures 5A and 6A, interactions between subunits in the S protein trimer were  
466 enhanced by receptor and trypsin treatment, and it remained stable in sample buffer  
467 containing 0.5% SDS during SDS-PAGE. To compare the strength of intermolecular  
468 interactions within the trimer at each step during the conformational changes, reactions of  
469 virus treated with receptor and trypsin were frozen at the indicated time points using dry  
470 ice/methanol, mixed with sample buffer containing trypsin inhibitor and 0.5% SDS, and  
471 incubated at different temperatures between 25°C and 100°C at intervals of 5°C. Both the  
472 trimer and the dissociated monomer were detected via western blotting following soaking of  
473 the PVDF membrane in stripping buffer used for trimer detection by MAb-10G. As shown in  
474 Figure 9A, the non-treated trimer in the pre-fusion state dissociated into the monomeric form  
475 at 25°C. After receptor binding, the dissociation temperature was increased to ~60°C. The  
476 dissociation temperature of the trimer was further increased to 90°C after trypsin treatment,  
477 and finally reached 95°C after 32 min (Fig. 9B).

478 Next, to explore the interactions of the three S2 subunits in more detail after the  
479 protease digestion step, experiments were performed between 81°C and 95°C at intervals of  
480 1°C, and the results of western blot analysis were cropped and aligned to compare the  
481 dissociated monomers (Fig. 9C). After trypsin treatment on ice, the dissociation temperature  
482 was ~85°C, and this gradually increased to 94°C during incubation, corresponding with the  
483 appearance of the 67 kDa fragment. These results indicate that the three S2 subunits in the  
484 trimer partially assemble at the receptor-binding step, and their interaction is dramatically  
485 enhanced by trypsin treatment. The postS2' site is finally cleaved after assembly.

486

#### 487 **Negative-stain EM**

488 Each virus activation step described above was visualized by negative-stain EM (Fig. 10A),  
489 and enlarged views of images are shown in Figure 10B. For non-treated virus, intact S protein  
490 globules were observed as uniform alignments on the viral membrane (Fig. 10B i). The  
491 height (distance) from the viral membrane to the top of the S protein was measured and is  
492 presented as a histogram (Fig. 10C). The height of uniform non-treated S protein was ~240  
493 Å, but after receptor treatment, the shapes of S proteins became more variable, gaps between  
494 S protein globules and the viral membrane were reduced (Fig. 10B ii), and the height of half  
495 of the S protein population was decreased to <200 Å (Fig. 10C ii). After trypsin treatment for  
496 5 min on ice, the S1 subunits appeared to remain on the S2 subunit, their shapes became  
497 obscured, and the gaps were further reduced (Fig. 10B iii and 10C iii). At 1 min after  
498 warming at 37°C, a few elongated cone-like structures were observed (Fig. 10B iv), as  
499 previously reported using recombinant S2 subunit (11). After additional incubation at 37°C  
500 for 30 min, almost all S protein globules disappeared, and many elongated cone-like  
501 structures appeared (Fig. 10A v and 10B v).

502 Next, the virus activation steps described above were probed in the presence of  
503 liposomes. On EM grids, an excessive number of liposomes but very few viruses were  
504 observed in the absence of soluble receptor (Fig. 10D i), whereas many virus particles were  
505 observed on liposomes in the presence of soluble receptor (Fig. 10D ii). These results  
506 correspond to liposome flotation assays in a previous study in which virus binding to  
507 liposomes was induced by receptor (26). Virus particles disappeared at 1 min after trypsin  
508 treatment (Fig. 10D iv), and fused liposomes were the dominant species observed at 30 min  
509 (Fig. 10D v), suggesting that membrane fusion with liposomes was largely complete within 1  
510 min, and liposomes then fused with each other using the remaining S protein. An enlarged  
511 view of virus-bound liposomes shown in Figure 10D ii and 10D iii is presented in Figure 10E.  
512 The gaps between viruses and liposomes that are presumably bridged by S protein were ~200  
513 Å after the receptor-binding step (Fig. 10E ii), and this distance was reduced by trypsin  
514 treatment on ice (Fig. 10E iii). A hazy density was evident between viruses and liposomes  
515 (Fig. 10E).

516

### 517 Discussion

518 The S protein of the MHV-2 virion is uncleaved, similar to the S protein of MERS-CoV and  
519 SARS-CoV, which requires cellular protease following receptor binding to induce S1  
520 dissociation from S2 and the subsequent conformational changes necessary for membrane  
521 fusion (26). By contrast, most MHV variants carry S proteins that are cleaved by cellular  
522 furin at the S1/S2 site during biogenesis, which was believed to require only receptor binding  
523 to induce membrane fusion (39, 40). However, previous studies of MHV and MERS-CoV  
524 suggest that the coronaviruses harboring pre-cleaved S protein (cleaved by furin during  
525 biogenesis) at the S1/S2 site require further cellular proteases to facilitate cell entry (20, 30).  
526 Our results also suggest that the S protein cleaved during biogenesis by furin requires

527 additional cleavage to induce conformational changes required to adopt a proteinase K-  
528 resistant conformation (Fig. 2A, lane 12). However, the trypsin-treated S protein cleaved on  
529 virus particles at the S1/S2 site does not require additional cleavage; it needs only receptor  
530 binding (Fig. 2A, lane 7). Therefore, these two types of S protein cleaved at the S1/S2 site are  
531 predicted to have different conformations. In the present study using MHV-2, the 67 and 69  
532 kDa products were considered to be by-products that reflect intermediate conformations of  
533 the S protein, although importance of cleavage at the S2' site was reported for coronavirus S  
534 proteins (20, 30).

535 Previous studies used cryoEM to examine conformational changes within the  
536 coronavirus S protein during the priming stage, which is induced by receptor binding; the  
537 results observed after receptor binding indicated an asymmetric trimer with opened and  
538 closed domains within the S1 subunit and a tightly assembled central helix in the S2 subunits  
539 (4, 6). However, no major differences in the HR region were observed. Although structural  
540 analysis using cryoEM is excellent for detecting stable protein structures, unstable structures  
541 such as the HR2 motifs in the S2 subunit cannot be analyzed using this technique, even if a  
542 large number of protein particles are captured; population-based biochemical analysis is  
543 needed to capture features of unstable proteins. Herein, we predicted the dynamic  
544 rearrangements of S2 subunits underpinning the transition from pre- to post-fusion structures  
545 based on western blot analysis of the 67 and 69 kDa by-products that are induced following  
546 trypsin digestion of the S protein.

547 Our model of the S protein conformational changes was constructed based on  
548 previously reported pre- and post-fusion structures (protein data bank codes 3JCL and 6B3O,  
549 respectively). The S2 subunit of coronavirus features a topology similar to that of the  
550 paramyxovirus F protein, comprising a core  $\beta$ -sheet, an upstream helix, and a central helix,  
551 and these motifs are essentially identical in pre- and post-fusion F protein structures (10, 41).

552 These invariant MHV-2 S protein motifs are assumed not to change conformation, and are  
553 displayed as a fixed globule represented by a gray column in Figure 11. The flexible regions  
554 in the S2 subunit that undergo conformational changes are positioned in the FP region  
555 (residues 867–949) and the HR1 region (residues 954–1072), as shown in Figure 4A and 4B.  
556 In addition, the region downstream of the core  $\beta$ -sheet (residues 1155–1302) that includes the  
557 HR2 region also appears to be flexible (Fig. 4A and 4B).

558 In the present and previous studies, we observed eight features related to  
559 conformational changes that occur in the flexible regions of the S2 subunit. The first four  
560 features are induced by receptor binding. [1] During this step, the S protein binds to the target  
561 membrane, as demonstrated by liposome-binding assays in a previous study (26) and  
562 negative-stain EM in this study (Fig. 10D ii). Because the FP region is located close to  $\beta$ 48,  
563 at least one  $\beta$ 48 per trimer must be dissociated from  $\beta$ 47 in invariant motifs for the FP region  
564 to be free. It is important to remember that the exact location of the FP region of coronavirus  
565 S protein remains controversial. The FP region (residues 867–949) immediately follows an  
566 S2' cleavage site (42), and another possible FP region (pFP; residues 967–983) is adjacent to  
567 the region upstream of HR1 (Fig. 4A and 4B), as reported previously (43, 44). [2] The  
568 metastable form of the S protein trimer is converted to a stable trimer (Fig. 6A, VHCR, lane  
569 3), for which the dissociation temperature was increased from 25°C to 60°C (Fig. 9C).  
570 During this stage, the movement of HR1 to form a trimeric  $\alpha$ -helical coiled-coil on the distal  
571 side of the viral membrane is restricted because the S2 subunit is still covered by the S1  
572 subunit in the uncleaved S protein (Fig. 10A ii). Therefore, regions at  $\alpha$ 29 and  $\alpha$ 30 (the  
573 central helix) are only capable of interacting within the trimer (Fig. 4B). This is consistent  
574 with a previous study in which the tightly packed central helix in the S2 subunit was detected  
575 by cryoEM after the receptor-binding step (4, 6). [3] The 106 amino acids of the connector  
576 region (residues 1155–1260, Fig. 4A), including the 10G epitope and disulfide bond at

577 positions 1169 and 1214, presumably form a folded structure because the 10G epitope in the  
578 trimer was undetectable in the native blot (Fig. 6A, 10G, lane 3), and was resistant to trypsin  
579 even in the presence of HR2-mimicking peptide (Fig. 8A). Reduction of the gap between the  
580 S protein globule and the viral membrane ( $\sim 200$  Å) in EM images (Fig. 10B ii and 10C ii)  
581 may reflect a folded C-terminal side of the S2 subunit. In addition, the 10G region is likely  
582 fixed near helix  $\alpha 29$  at the top of the S2 trimer to allow 6HB assembly in the following step  
583 (11). These observations indicate that, in the S protein structure appearing after the receptor-  
584 binding step, the core of the connector leash is packed into the groove of the invariant motif  
585 (Fig. 11A ii, purple lines), as seen in the post-fusion structure (11). [4] The HR1/HR2 motif  
586 forms the packed-hairpin structure observed as the 67 kDa subunit after trypsin treatment that  
587 is unable to interact with HR2-mimicking peptide (Fig. 8A, lane 13 and 8G, lane 2). Based on  
588 the steric configuration of the post-fusion structure, HR1 of one S2 subunit must be packed  
589 with HR2 of another S2 subunit in the trimer to form a hairpin structure (11). Additionally,  
590 unpacked HR1, observed as the 69 kDa band that was degraded following treatment with  
591 HR2-mimicking peptide and trypsin (Fig. 8G, lane 2), also appeared in this step.  
592 Interestingly, both 69 and 67 kDa subunits were present in the trimer, as revealed by two-  
593 dimensional electrophoresis (Fig. 5C b), suggesting that a subset of S2 subunits form a  
594 heterogeneous trimer constructed from two different conformational states. We predict that  
595 the trimer includes at least one packed HR1/HR2 motif and extends at least one unpacked  
596 HR1 motif toward the target membrane to expose the FP region, and the S2 subunit is  
597 covered by the S1 subunit in the uncleaved S protein (Fig. 11A ii). These features suggest  
598 that the S protein cannot form the typical homotrimeric pre-hairpin structure predicted in the  
599 current model of class I viral fusion protein assembly (Fig. 11B).

600 The next four features of the conformational changes are induced by trypsin  
601 treatment, during which obscure-shaped S proteins were observed by EM (Fig. 10B iii). [5]

602 The S1/S2 site is cleaved by trypsin to generate the 90 kDa subunit (Fig. 1C, lane 7 and 7A,  
603 lane 2), and the S2' site is subsequently cleaved by trypsin to generate the 69 kDa subunit  
604 (Fig. 1C, lanes 7–16). Release of the S1 subunit from the S2 subunit presumably enhances  
605 interactions within three S2 subunits and triggers conformational changes in the HR1/HR2  
606 motifs. [6] All three HR1/HR2 motifs in the trimer appear to form a packed-hairpin structure  
607 at 1 min after warming at 37°C because HR2-mimicking peptide cannot interact with them  
608 (Fig. 8G, lane 3). [7] Simultaneously, the three HR1/HR2 motifs assemble at the center to  
609 form a 6HB core at 1 min after trypsin treatment (Fig. 7A, bottom, lane 3). At this stage, the  
610 dissociation temperature of the trimer was ~90°C (Fig. 9C). [8] The postS2' cleavage site in  
611  $\beta$ 48 is finally cleaved by trypsin after assembly of the three HR motifs at the center, resulting  
612 in the appearance of the 67 kDa subunit (Fig. 9C bottom). The final 6HB structure is  
613 constructed from 67 and 69 kDa subunits or three 67 kDa subunits (Fig. 5C b). Numerous  
614 elongated cone-like structures were observed by EM (Fig. 10A v).

615 As described above, at least one HR1/HR2 motif per trimer may form a packed-  
616 hairpin structure after the receptor-binding step, and another exposes the FP region, as  
617 illustrated in Figure 11A ii. This conformation presumably facilitates formation of an  
618 asymmetric trimer. In principle, the class I viral fusion protein trimer must break its rotational  
619 symmetry during activation to overcome the steric hindrance within the three fusion protein  
620 subunits (45, 46). When the different conformational states of the HR1/HR2 motif assemble  
621 in the trimer, the axis of the trimer is presumably tilted against the viral membrane (Fig. 11A  
622 vii), resulting in the breaking of rotational symmetry. This is followed by formation of 6HB  
623 and membrane fusion. Flexibility at the juxtamembrane region and the tilted orientation  
624 against the viral membrane required for membrane fusion were recently reported by a study  
625 examining influenza HA in detergent micelles analyzed by cryoEM (47). We anticipate that

626 the mechanism suggested by western blot analysis herein will be confirmed by other  
627 approaches such as high-resolution cryoEM and/or *in silico* simulation.

628

629

630

### 631 **Acknowledgments**

632 We thank Judith M. White (Virginia University) for valuable suggestions about this work,  
633 and Fumihiko Taguchi (Chungnam National University) for providing an opportunity to work  
634 on this project. We also thank Noriyo Nagata (NIID) for technical suggestions, and Berend-  
635 Jan Bosch and Peter J. M. Rottier (Utrecht University) for providing HR2-mimicking peptide.

636

### 637 **Funding**

638 This study was supported by a Grant-in-Aid for Scientific Research from the Japan Society  
639 for the Promotion of Science (Grant No. 17864517).

640

### 641 **References**

- 642 1. White JM, Whittaker GR. 2016. Fusion of Enveloped Viruses in Endosomes. *Traffic*  
643 17:593–614.
- 644 2. Heald-Sargent T, Gallagher T. 2012. Ready, set, fuse! the coronavirus spike protein  
645 and acquisition of fusion competence. *Viruses* 4:557–580.
- 646 3. Harrison SC. 2015. Viral membrane fusion. *Virology* 479–480:498–507.
- 647 4. Walls AC, Xiong X, Park YJ, Tortorici MA, Snijder J, Quispe J, Camerani E, Gopal  
648 R, Dai M, Lanzavecchia A, Zambon M, Rey FA, Corti D, Veasler D. 2019.  
649 Unexpected Receptor Functional Mimicry Elucidates Activation of Coronavirus  
650 Fusion. *Cell* 176:1026-1039.e15.

- 651 5. Ozorowski G, Pallesen J, De Val N, Lyumkis D, Cottrell CA, Torres JL, Copps J,  
652 Stanfield RL, Cupo A, Pugach P, Moore JP, Wilson IA, Ward AB. 2017. Open and  
653 closed structures reveal allostery and pliability in the HIV-1 envelope spike. *Nature*  
654 547:360–361.
- 655 6. Yuan Y, Cao D, Zhang Y, Ma J, Qi J, Wang Q, Lu G, Wu Y, Yan J, Shi Y, Zhang X,  
656 Gao GF. 2017. Cryo-EM structures of MERS-CoV and SARS-CoV spike  
657 glycoproteins reveal the dynamic receptor binding domains. *Nat Commun* 8:1–9.
- 658 7. Gui M, Song W, Zhou H, Xu J, Chen S, Xiang Y, Wang X. 2016. Cryo-electron  
659 microscopy structures of the SARS-CoV spike glycoprotein reveal a prerequisite  
660 conformational state for receptor binding. *Cell Res* 27:119–129.
- 661 8. Kirchdoerfer RN, Wang N, Pallesen J, Wrapp D, Turner HL, Cottrell CA, Corbett KS,  
662 Graham BS, McLellan JS, Ward AB. 2018. Stabilized coronavirus spikes are resistant  
663 to conformational changes induced by receptor recognition or proteolysis. *Sci Rep*  
664 8:15701.
- 665 9. Lee M, Yao H, Kwon B, Waring AJ, Ruchala P, Singh C, Hong M. 2018.  
666 Conformation and Trimer Association of the Transmembrane Domain of the  
667 Parainfluenza Virus Fusion Protein in Lipid Bilayers from Solid-State NMR: Insights  
668 into the Sequence Determinants of Trimer Structure and Fusion Activity. *J Mol Biol*  
669 430:695–709.
- 670 10. Walls AC, Tortorici MA, Bosch B-J, Frenz B, Rottier PJM, DiMaio F, Rey F a.,  
671 Veesler D. 2016. Cryo-electron microscopy structure of a coronavirus spike  
672 glycoprotein trimer. *Nature* 531:114–117.
- 673 11. Walls AC, Tortorici MA, Snijder J, Xiong X, Bosch B, Rey FA. 2017. Tectonic  
674 conformational changes of a coronavirus spike glycoprotein promote membrane  
675 fusion. *Proc Natl Acad Sci* 114:11157–11162.

- 676 12. Kirchdoerfer RN, Cottrell CA, Wang N, Pallesen J, Yassine HM, Turner HL, Corbett  
677 KS, Graham BS, McLellan JS, Ward AB. 2016. Prefusion structure of a human  
678 coronavirus spike protein. *Nature* 531:118–121.
- 679 13. Pallesen J, Wang N, Corbett KS, Wrapp D, Kirchdoerfer RN, Turner HL, Cottrell CA,  
680 Becker MM, Wang L, Shi W, Kong W-P, Andres EL, Kettenbach AN, Denison MR,  
681 Chappell JD, Graham BS, Ward AB, McLellan JS. 2017. Immunogenicity and  
682 structures of a rationally designed prefusion MERS-CoV spike antigen. *Proc Natl*  
683 *Acad Sci U S A* 114:E7348–E7357.
- 684 14. Lee KK. 2010. Architecture of a nascent viral fusion pore. *EMBO J* 29:1299–1311.
- 685 15. Maurer UE, Sodeik B, Grünewald K. 2008. Native 3D intermediates of membrane  
686 fusion in herpes simplex virus 1 entry. *Proc Natl Acad Sci U S A* 105:10559–64.
- 687 16. Riedel C, Vasishtan D, Siebert CA, Whittle C, Lehmann MJ, Mothes W, Grünewald  
688 K. 2017. Native structure of a retroviral envelope protein and its conformational  
689 change upon interaction with the target cell. *J Struct Biol* 197:172–180.
- 690 17. Sjöberg M, Löving R, Lindqvist B, Garoff H. 2017. Sequential activation of the three  
691 protomers in the Moloney murine leukemia virus Env. *Proc Natl Acad Sci U S A*  
692 114:2723–2728.
- 693 18. Gierer S, Bertram S, Kaup F, Wrensch F, Heurich A, Krämer-Kühl A, Welsch K,  
694 Winkler M, Meyer B, Drosten C, Dittmer U, von Hahn T, Simmons G, Hofmann H,  
695 Pöhlmann S. 2013. The spike protein of the emerging betacoronavirus EMC uses a  
696 novel coronavirus receptor for entry, can be activated by TMPRSS2, and is targeted by  
697 neutralizing antibodies. *J Virol* 87:5502–11.
- 698 19. Haan CAM De, Stadler K, Godeke G, Bosch BJ, Rottier PJM. 2004. Cleavage  
699 Inhibition of the Murine Coronavirus Spike Protein by a Furin-Like Enzyme Affects  
700 Cell-Cell but Not Virus-Cell Fusion. *J Virol* 78:6048–6054.

- 701 20. Park J-E, Li K, Barlan A, Fehr AR, Perlman S, McCray PB, Gallagher T. 2016.  
702 Proteolytic processing of Middle East respiratory syndrome coronavirus spikes  
703 expands virus tropism. *Proc Natl Acad Sci U S A* 113:12262–12267.
- 704 21. Reinke LM, Spiegel M, Plegge T, Hartleib A, Nehlmeier I, Gierer S, Hoffmann M,  
705 Hofmann-winkler H, Winkler M, Pöhlmann S. 2017. Different residues in the SARS-  
706 CoV spike protein determine cleavage and activation by the host cell protease  
707 TMPRSS2. *PLoS One* 12(6):e0179177.
- 708 22. Belouzard S, Millet JK, Licitra BN, Whittaker GR. 2012. Mechanisms of coronavirus  
709 cell entry mediated by the viral spike protein. *Viruses* 4:1011–1033.
- 710 23. Zheng Y, Shang J, Yang Y, Liu C, Wan Y, Geng Q, Wang M, Baric R, Li F. 2018.  
711 Lysosomal Proteases Are a Determinant of Coronavirus Tropism. *J Virol* 92:e01504-  
712 18.
- 713 24. Kawase M, Shirato K, Matsuyama S, Taguchi F. 2009. Protease-mediated entry via the  
714 endosome of human coronavirus 229E. *J Virol* 83:712–721.
- 715 25. Simmons G, Reeves JD, Rennekamp AJ, Amberg SM, Piefer AJ, Bates P. 2004.  
716 Characterization of severe acute respiratory syndrome-associated coronavirus (SARS-  
717 CoV) spike glycoprotein-mediated viral entry. *Proc Natl Acad Sci U S A* 101:4240–  
718 4245.
- 719 26. Matsuyama S, Taguchi F. 2009. Two-step conformational changes in a coronavirus  
720 envelope glycoprotein mediated by receptor binding and proteolysis. *J Virol*  
721 83:11133–11141.
- 722 27. Belouzard S, Chu VC, Whittaker GR. 2009. Activation of the SARS coronavirus spike  
723 protein via sequential proteolytic cleavage at two distinct sites. *Proc Natl Acad Sci U S*  
724 *A* 106:5871–5876.

- 725 28. Watanabe R, Matsuyama S, Shirato K, Maejima M, Fukushi S, Morikawa S, Taguchi  
726 F. 2008. Entry from the cell surface of severe acute respiratory syndrome coronavirus  
727 with cleaved S protein as revealed by pseudotype virus bearing cleaved S protein. *J*  
728 *Virology* 82:11985–11991.
- 729 29. Yamada YK, Takimoto K, Yabe M, Taguchi F. 1997. Acquired fusion activity of a  
730 murine coronavirus MHV-2 variant with mutations in the proteolytic cleavage site and  
731 the signal sequence of the S protein. *Virology* 227:215–219.
- 732 30. Burkard C, Verheije MH, Wicht O, van Kasteren SI, van Kuppeveld FJ, Haagsmans  
733 BL, Pelkmans L, Rottier PJM, Bosch BJ, de Haan C a. M. 2014. Coronavirus Cell  
734 Entry Occurs through the Endo-/Lysosomal Pathway in a Proteolysis-Dependent  
735 Manner. *PLoS Pathog* 10:e1004502.
- 736 31. Wicht O, Burkard C, de Haan CAM, van Kuppeveld FJM, Rottier PJM, Bosch BJ.  
737 2014. Identification and Characterization of a Proteolytically Primed Form of the  
738 Murine Coronavirus Spike Proteins after Fusion with the Target Cell. *J Virol* 88:4943–  
739 4952.
- 740 32. Millet JK, Whittaker GR. 2014. Host cell entry of Middle East respiratory syndrome  
741 coronavirus after two-step, furin-mediated activation of the spike protein. *Proc Natl*  
742 *Acad Sci U S A* 111:15214–9.
- 743 33. Matsuyama S, Shirato K, Kawase M, Terada Y, Kawachi K, Fukushi S, Kamitani W.  
744 2018. Middle East Respiratory Syndrome Coronavirus Spike Protein Is Not Activated  
745 Directly by Cellular Furin during Viral Entry into Target Cells. *J Virol* 92:1–12.
- 746 34. Hirano N, Fujiwara K, Hino S, Matumoto M. 1974. Replication and plaque formation  
747 of mouse hepatitis virus (MHV-2) in mouse cell line DBT culture. *Arch Gesamte*  
748 *Virusforsch* 44:298–302.

- 749 35. Matsuyama S, Taguchi F. 2002. Receptor-Induced Conformational Changes of Murine  
750 Coronavirus Spike Protein. *J Virol* 76:11819–11826.
- 751 36. Bosch BJ, Rossen JWA, Bartelink W, Zuurveen SJ, de Haan CAM, Duquerroy S,  
752 Boucher CAB, Rottier PJM. 2008. Coronavirus Escape from Heptad Repeat 2 (HR2)-  
753 Derived Peptide Entry Inhibition as a Result of Mutations in the HR1 Domain of the  
754 Spike Fusion Protein. *J Virol* 82:2580–2585.
- 755 37. Taguchi F, Shimazaki YK. 2000. Functional analysis of an epitope in the S2 subunit of  
756 the murine coronavirus spike protein: Involvement in fusion activity. *J Gen Virol*  
757 81:2867–2871.
- 758 38. Ujike M, Nishikawa H, Otaka A, Yamamoto N, Yamamoto N, Matsuoka M, Kodama  
759 E, Fujii N, Taguchi F. 2007. Heptad Repeat-Derived Peptides Block Protease-  
760 Mediated Direct Entry from the Cell Surface of Severe Acute Respiratory Syndrome  
761 Coronavirus but Not Entry via the Endosomal Pathway. *J Virol* 82:588–592.
- 762 39. Sturman LS, Ricard CS, Holmes K V. 1990. Conformational change of the coronavirus  
763 peplomer glycoprotein at pH 8.0 and 37 degrees C correlates with virus aggregation  
764 and virus-induced cell fusion. *J Virol* 64:3042–50.
- 765 40. Gallagher TM. 1997. A role for naturally occurring variation of the murine coronavirus  
766 spike protein in stabilizing association with the cellular receptor. *J Virol* 71:3129–37.
- 767 41. McLellan JS, Yang Y, Graham BS, Kwong PD. 2011. No TitleStructure of Respiratory  
768 Syncytial Virus Fusion Glycoprotein in the Postfusion Conformation Reveals  
769 Preservation of Neutralizing Epitopes. *J Virol* 85:7788–7796.
- 770 42. Madu IG, Roth SL, Belouzard S, Whittaker GR. 2009. Characterization of a highly  
771 conserved domain within the severe acute respiratory syndrome coronavirus spike  
772 protein S2 domain with characteristics of a viral fusion peptide. *J Virol* 83:7411–7421.

- 773 43. Ou X, Zheng W, Shan Y, Mu Z, Dominguez SR, Holmes K V., Qian Z. 2016.  
774 Identification of the Fusion Peptide-Containing Region in Betacoronavirus Spike  
775 Glycoproteins. *J Virol* 90:5586–5600.
- 776 44. Luo Z, Weiss SR. 1998. Roles in cell-to-cell fusion of two conserved hydrophobic  
777 regions in the murine coronavirus spike protein. *Virology* 244:483–494.
- 778 45. von Messling V, Milosevic D, Devaux P, Cattaneo R. 2004. Canine distemper virus  
779 and measles virus fusion glycoprotein trimers: partial membrane-proximal ectodomain  
780 cleavage enhances function. *J Virol* 78:7894–7903.
- 781 46. Cohen FS, Melikyan GB. 2004. The energetics of membrane fusion from binding,  
782 through hemifusion, pore formation, and pore enlargement. *J Membr Biol* 199:1–14.
- 783 47. Benton DJ, Nans A, Calder LJ, Turner J, Neu U, Lin YP, Ketelaars E, Kallewaard NL,  
784 Corti D, Lanzavecchia A, Gamblin SJ, Rosenthal PB, Skehel JJ. 2018. Influenza  
785 hemagglutinin membrane anchor. *Proc Natl Acad Sci* 115:10112–10117.
- 786  
787

## 788 **Figure Legends**

789 **Fig. 1. Proteolytic activation of the MHV-2 spike (S) protein.** (A) Schematic diagram of  
790 MHV-2 S protein organization. Letters A, B, C, and D indicate domains of the S1 subunit.  
791 SP, signal peptide; RBD, receptor-binding domain; UH, upstream helix; FP, fusion peptide;  
792 HR1/HR2, heptad repeats; CH, central helix; BH,  $\beta$ -hairpin; CR, connector region; TMD,  
793 transmembrane domain. The three trypsin cleavage sites are indicated by black arrows, and  
794 the four linear epitopes recognized by antibodies are indicated by white arrows. (B) Two-step  
795 conformational changes of S protein primed by receptor binding and triggered by trypsin.  
796 MHV-2 pre-treated with a soluble form of the receptor (CEACAM1a, receptor) was  
797 incubated with trypsin (10  $\mu$ g/ml). Samples were boiled and subjected to western blot

798 analysis using the indicated antibodies. (C) Trypsin concentration-dependent cleavage of S  
799 protein. MHV-2 pre-treated with receptor was incubated with various concentrations of  
800 trypsin, then with proteinase K. Samples were boiled and subjected to western blot analysis  
801 using MAb-10G antibody. (D) Trypsin concentration dependence of virus cell entry. MHV-2  
802 was adsorbed onto DBT cells, and various concentrations of trypsin were added. After a 5 h  
803 incubation, viral mRNA was quantified by real-time PCR (n = 6). Data were analyzed  
804 relative to the no trypsin control using two-tailed Student's t-tests. n.s. = not significant, \* =  
805 significant ( $p \leq 0.05$ ), \*\* = highly significant ( $p \leq 0.01$ ), \*\*\* = very highly significant  
806 ( $p \leq 0.001$ ). Error bars indicate standard deviation (SD).

807

808 **Fig. 2. Proteolytic activation of the pre-cleaved S protein.** (A) Conformational changes in  
809 pre-cleaved S proteins. To prepare the virus harboring a cleaved S protein, MHV-2 was  
810 treated with 1  $\mu\text{g/ml}$  trypsin or phosphate-buffered saline (PBS) (uncleaved control) for 1 h,  
811 treated with trypsin inhibitors, and then purified on a Sephadex G-75 column.

812 Conformational changes in PBS-treated MHV-2, trypsin-treated MHV-2, and MHV-2f  
813 harboring a pre-cleaved S protein were examined as described in Figure 1. Samples were  
814 boiled and subjected to western blot analysis with MAb-10G antibody. (B) Cell entry by  
815 viruses. Viruses treated with PBS or trypsin were inoculated onto DBT cells, and cellular  
816 RNA was isolated after 0 or 6 h. Viral mRNA was quantified by real-time PCR (n = 4).

817

818 **Fig. 3. Additional characterization of the 67 and 69 kDa subunits.** (A) Specific cleavage  
819 of the postS2' site at arginine or lysine residues. Endopeptidase arg-C (20  $\mu\text{g/ml}$ ) and/or lys-  
820 C (20  $\mu\text{g/ml}$ ) were employed instead of trypsin to induce S protein conformational changes.  
821 (B) Deglycosylation of S2 subunits. S protein activated by receptor and trypsin was  
822 deglycosylated using a deglycosylation enzyme mix. Nonrelevant lanes on the same blot were

823 sliced out in Adobe Photoshop to align the lanes shown. (C) Receptor concentration  
824 dependence. MHV-2 was treated with serially diluted soluble receptor, then with trypsin (10  
825  $\mu\text{g/ml}$ ). (D) Effect of redox potential. The 67 and 69 kDa subunits induced by the treatment  
826 of receptor and trypsin (0.32 and 32  $\mu\text{g/ml}$ ) were boiled in sample buffer containing the  
827 indicated concentration of dithiothreitol (DTT). (A–D) After SDS-PAGE, western blot  
828 analysis was carried out using MAb-10G antibody.

829

830 **Fig. 4. Primary structure and topology of the MHV-2 S2 subunit.** (A) Primary sequence  
831 of the S2 subunit. Gray areas indicate invariant motifs present in both pre- and post-fusion  
832 structures. S-S, disulfide bridge; glyco, N-glycosylation site; scissor mark, trypsin cleavage  
833 site. The four antibody-binding sites and the functional motifs are depicted. (B) Topology of  
834 the pre-fusion form of S protein based on the cryoEM structure (10). Colors and labels  
835 correspond to those in panel A. Magenta dotted lines indicate molecular interactions between  
836 motifs.

837

838 **Fig. 5. Components of the S2 trimer after triggering.** (A) Comparison of native and  
839 denatured S protein. MHV-2 treated with soluble receptor and trypsin was divided into two  
840 aliquots for unboiled (native) and boiled (denatured) treatments. After electrophoresis on a  
841 3–10% gel, the gel was boiled in sample buffer at 105°C for 5 min in an autoclave, and  
842 transferred to a PVDF membrane. (B) Two-dimensional electrophoresis. The reaction  
843 mixture prepared as described for panel A was mixed with sample buffer containing  
844 molecular size markers, and two-dimensional electrophoresis was carried out. After the first  
845 electrophoresis step, the first gel (3–10%) was boiled in sample buffer, sliced along the  
846 markers, and laid onto the second gel (7.5%). After the second electrophoresis step, the gel  
847 was transferred to a PVDF membrane. X-marks indicate overlaid molecular size markers. (C)

848 Cropped and enlarged blots. Blots from two-dimensional electrophoresis and western blot  
849 analysis corresponding to 0.32 or 10  $\mu\text{g/ml}$  trypsin treatment were cropped at 67 and 69 kDa  
850 and enlarged by graphical manipulation software. (A–C) Western blot analysis was carried  
851 out using MAb-10G antibody.

852

853 **Fig. 6. Exposed or buried configurations of epitopes in the S protein globule.** (A) Native  
854 SDS-PAGE. Unboiled samples were subjected to western blot analysis. (B) Denaturing and  
855 re-probing. PVDF membranes from panel A were soaked in stripping buffer for 5 min to  
856 denature the bound S protein, and subjected to detection with the same antibodies a second  
857 time. (A and B) Western blot analysis was performed using the indicated antibodies.

858

859 **Fig. 7. Timing of the appearance of the 90, 69, 67, and 53 kDa species.** (A) Time course of  
860 90, 69, 67, and 53 kDa fragment generation. MHV-2 was treated with receptor and trypsin,  
861 and the reaction was stopped by freezing at the indicated time points. (B) Two-step  
862 conformational changes in the S protein primed by receptor binding and triggered by trypsin  
863 in the presence of liposomes. (C) Time course of the generation of 90, 69, and 67 kDa  
864 fragments in the presence of liposomes. MHV-2 was treated with receptor and trypsin in the  
865 presence of liposomes, and the reaction was stopped by freezing at the indicated time points.  
866 (A–C) Appearance of S2 subunits (90, 69, and 67 kDa) detected by western blot analysis  
867 using MAb-10G antibody.

868

869 **Fig. 8. Interaction of HR2-mimicking peptide with the S2 subunit.** (A) Effect of HR2-  
870 mimicking peptide (HR2-peptide) during S protein triggering. HR2-peptide (50  $\mu\text{M}$ ) was  
871 added to MHV-2 after the receptor-binding step, and reaction mixtures were treated with  
872 various concentrations of trypsin. (B) The PVDF membrane from panel A was re-probed with

873 anti-CT antibody. (C) Reaction mixtures from panel A were treated with proteinase K to  
874 generate the 53 kDa fragment. (D) Effect of trypsin on the HR2-peptide. HR2-peptide non-  
875 treated or pre-treated with 10  $\mu\text{g/ml}$  trypsin for 30 min was diluted and added to the reaction  
876 containing MHV-2 and receptor, and reaction mixtures were treated with 10  $\mu\text{g/ml}$  trypsin.  
877 (E) Reaction mixtures from panel D were treated with proteinase K to generate the 53 kDa  
878 fragment. (F) Blocking virus cell entry. MHV-2 was adsorbed onto DBT cells, and 10  $\mu\text{g/ml}$   
879 trypsin was added in the presence or absence of HR2-mimicking peptide. After a 5 h  
880 incubation, viral mRNA was quantified by real-time PCR ( $n = 6$ ). Data were analyzed  
881 relative to the no peptide control using two-tailed Student's t-tests, as described in the legend  
882 of Figure 1. (G) Time course of HR1/HR2 motif packing. During S protein activation by  
883 receptor and trypsin, the reaction was stopped by freezing at the indicated time points, and  
884 HR2-mimicking peptide (HR2-peptide) was added and incubated for 20 min to facilitate the  
885 formation of 67 and 69 kDa fragments. (A–E and G) Western blot analysis was performed  
886 using the indicated antibodies.

887

888 **Fig. 9. Timing of S2 subunit assembly.** (A) Thermostability of the trimer in the receptor-  
889 binding step. The reaction analyzing conformational changes of S protein was stopped by  
890 freezing at the indicated time points after 30 min treatment with receptor. (B) Thermostability  
891 of the trimer in the proteolysis step. Reaction mixtures prepared as described for panel A  
892 were treated with trypsin and stopped by freezing at the indicated time points. (C) More  
893 detailed analysis of S protein thermostability. The dissociation temperature of mixtures  
894 prepared as described for panel B was explored between 81°C and 95°C at intervals of 1°C.  
895 (A–C) Reaction mixtures were treated with sample buffer containing protease inhibitor and  
896 0.5% SDS on ice, then incubated at the indicated temperature using a Veriti thermal cycler  
897 (ThermoFisher). After electrophoresis and electroblotting, the PVDF membrane was soaked

898 in stripping buffer for trimer detection by MAb-10G. Dissociated monomer bands from each  
899 step of the conformational changes were cropped and aligned to compare the dissociation  
900 temperature in panel C.

901

902 **Fig. 10. Visualization by negative-stain electron microscopy (EM).** (A) Virus particles.  
903 MHV-2 treated with or without receptor (1  $\mu$ M) and trypsin (10  $\mu$ g/ml) to induce  
904 conformational changes in S protein was subjected to negative-stain EM. (B) Enlarged view  
905 of S protein on the viral particle. (C) Histogram of S protein height above the membrane. S  
906 proteins ( $n = 32$ ) in five viral particles were measured and represented as a histogram. (D)  
907 Visualization of virus binding to liposomes. Liposomes were added to the reaction to induce  
908 conformational changes in the viral S protein. Viruses are indicated by arrows. (E) Enlarged  
909 view of virus binding to liposomes. Virus particles observed in panel D are enlarged.

910

911 **Fig. 11. Schematic diagram of S protein activation.** (A) Conformational changes of the S  
912 protein trimer. (B) Homotrimeric pre-hairpin structure in the unified model of class I viral  
913 fusion protein assembly. FP, fusion peptide; HR1/HR2, heptad repeats.

914

Fig. 1

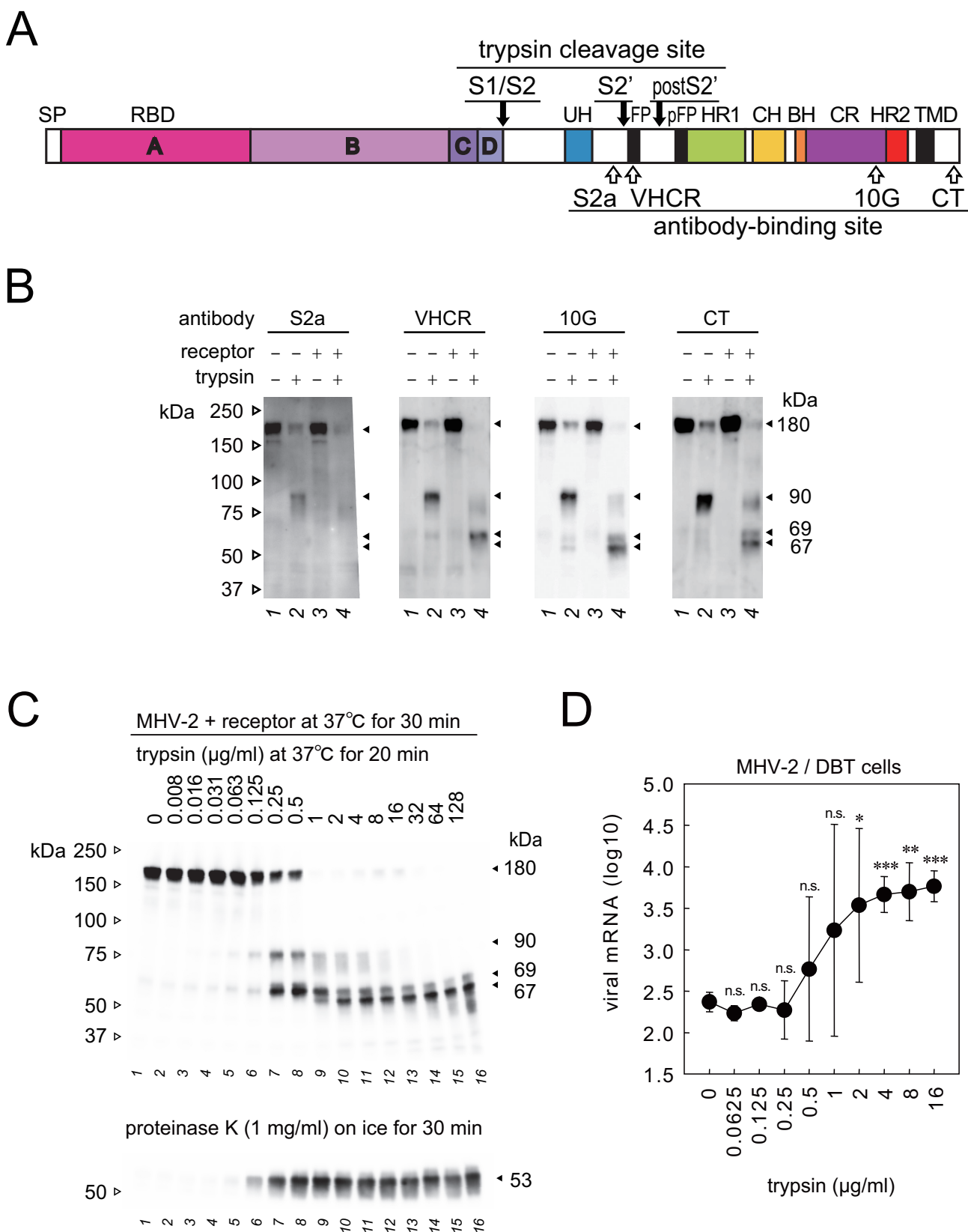


Fig. 2

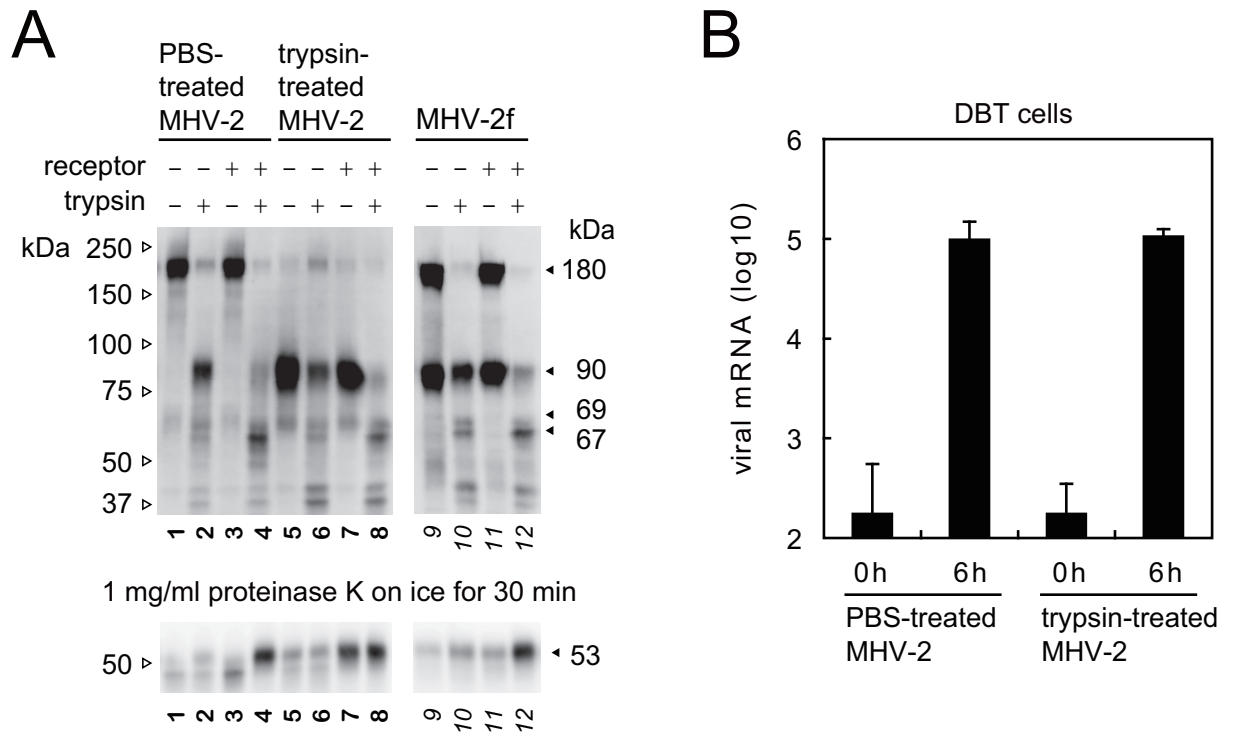


Fig. 3

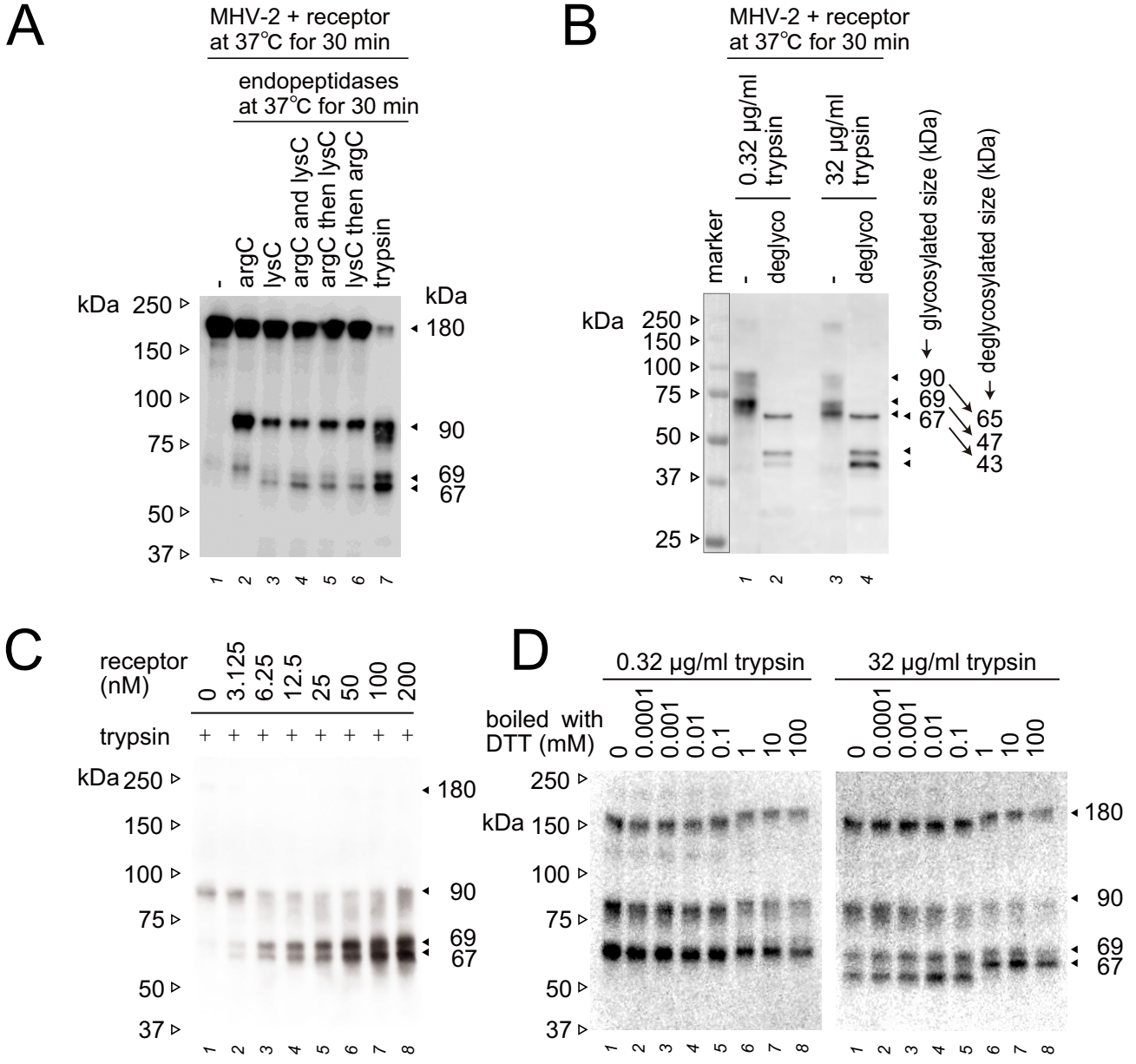
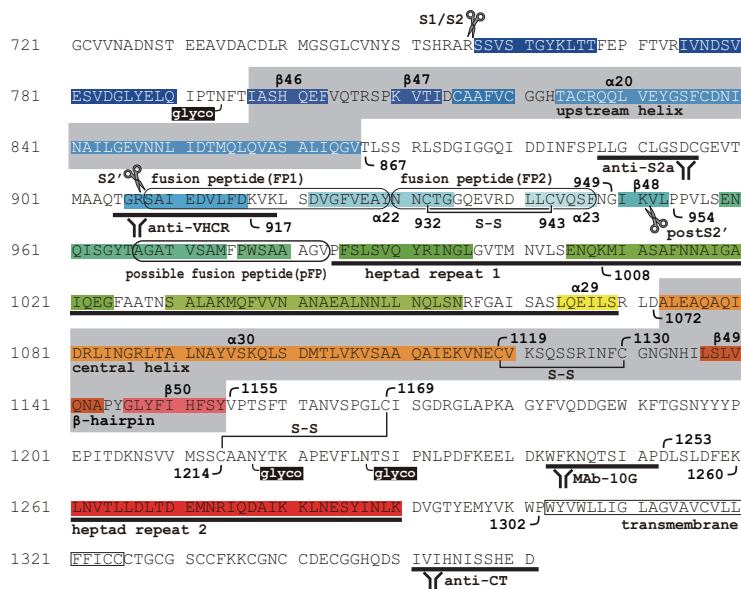


Fig. 4

A



B

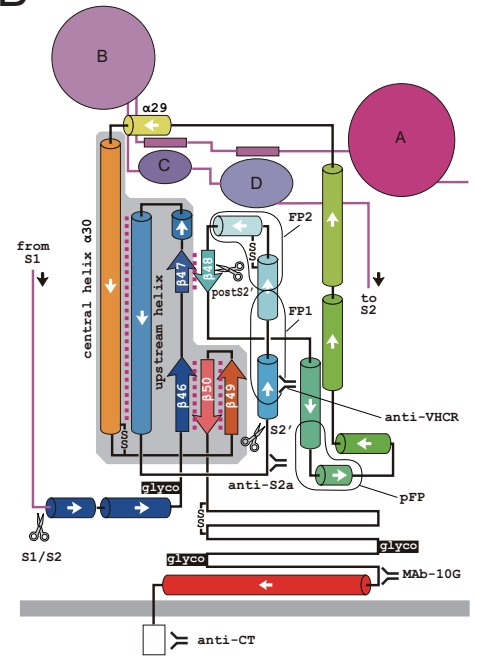


Fig. 5

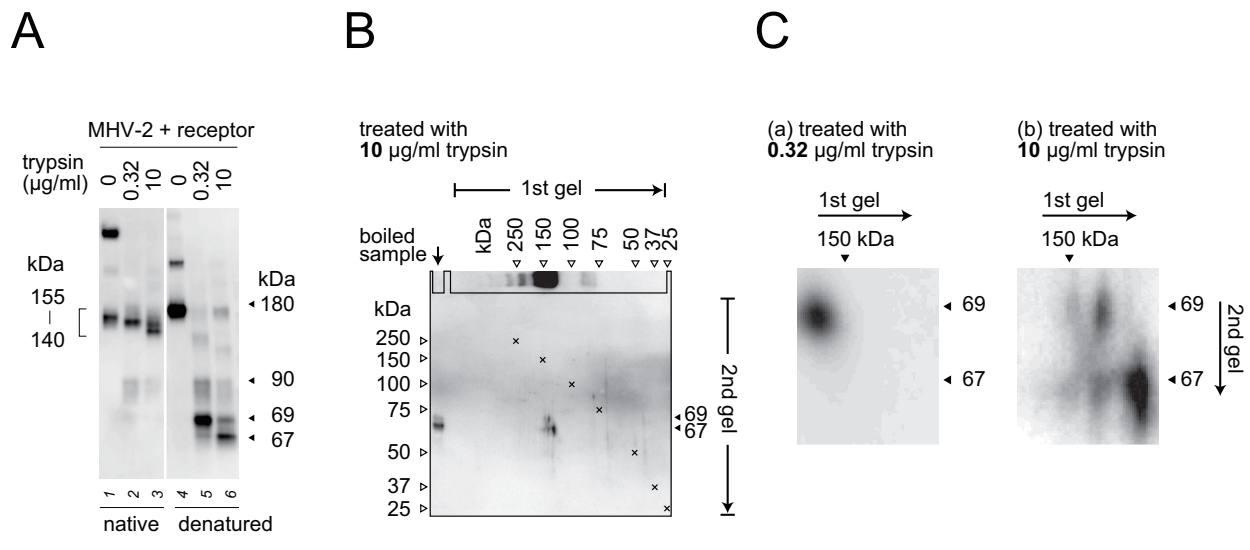


Fig. 6

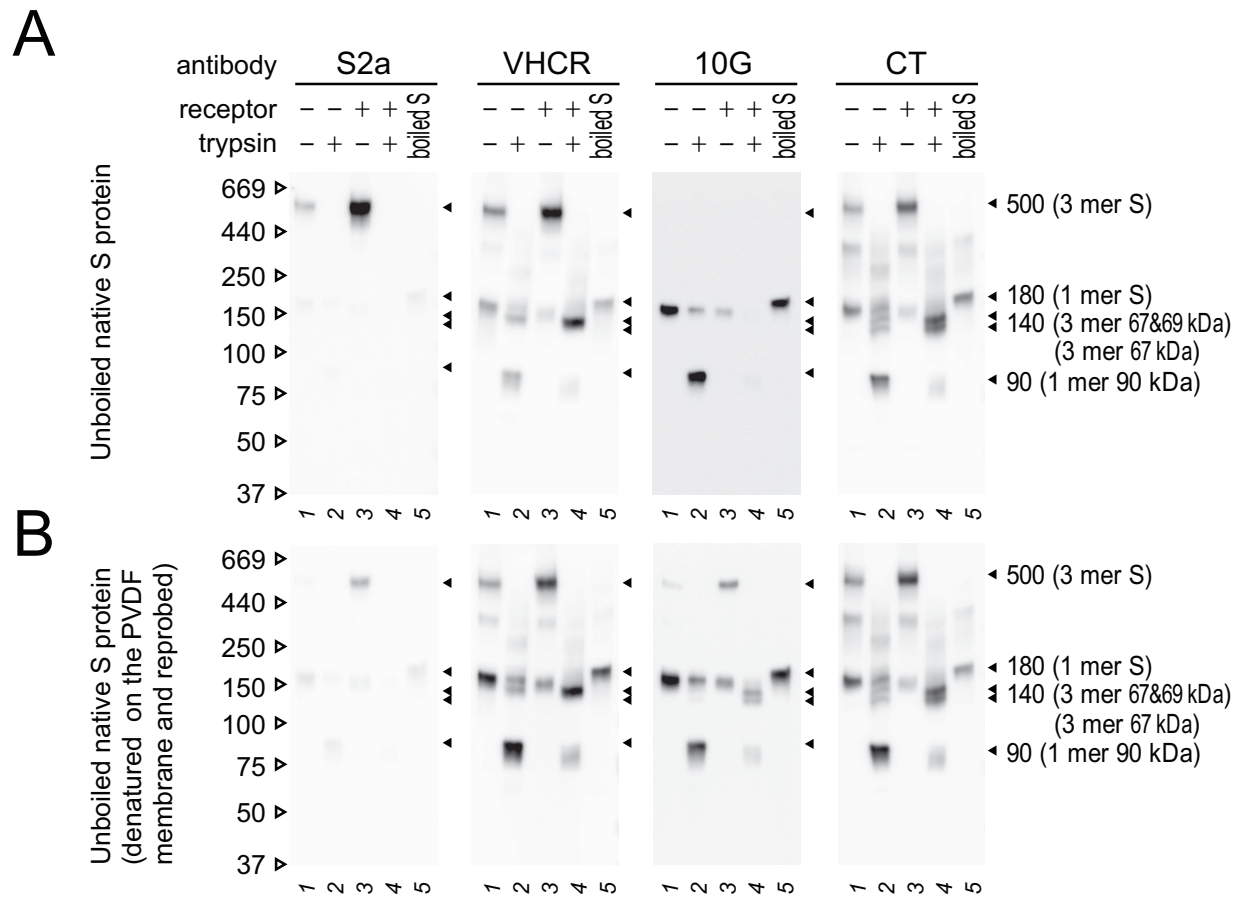


Fig. 7

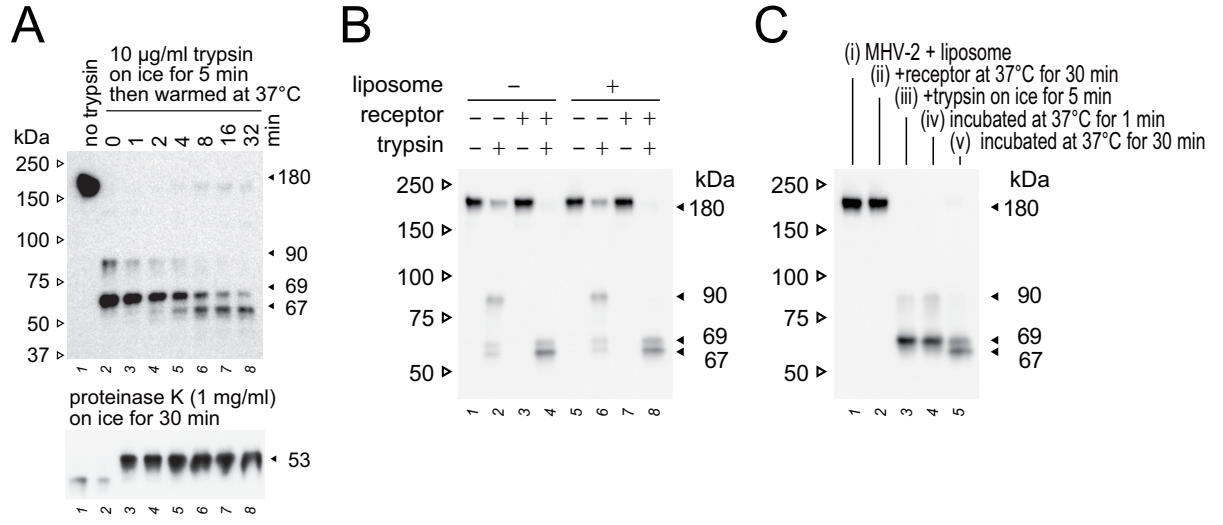


Fig. 8

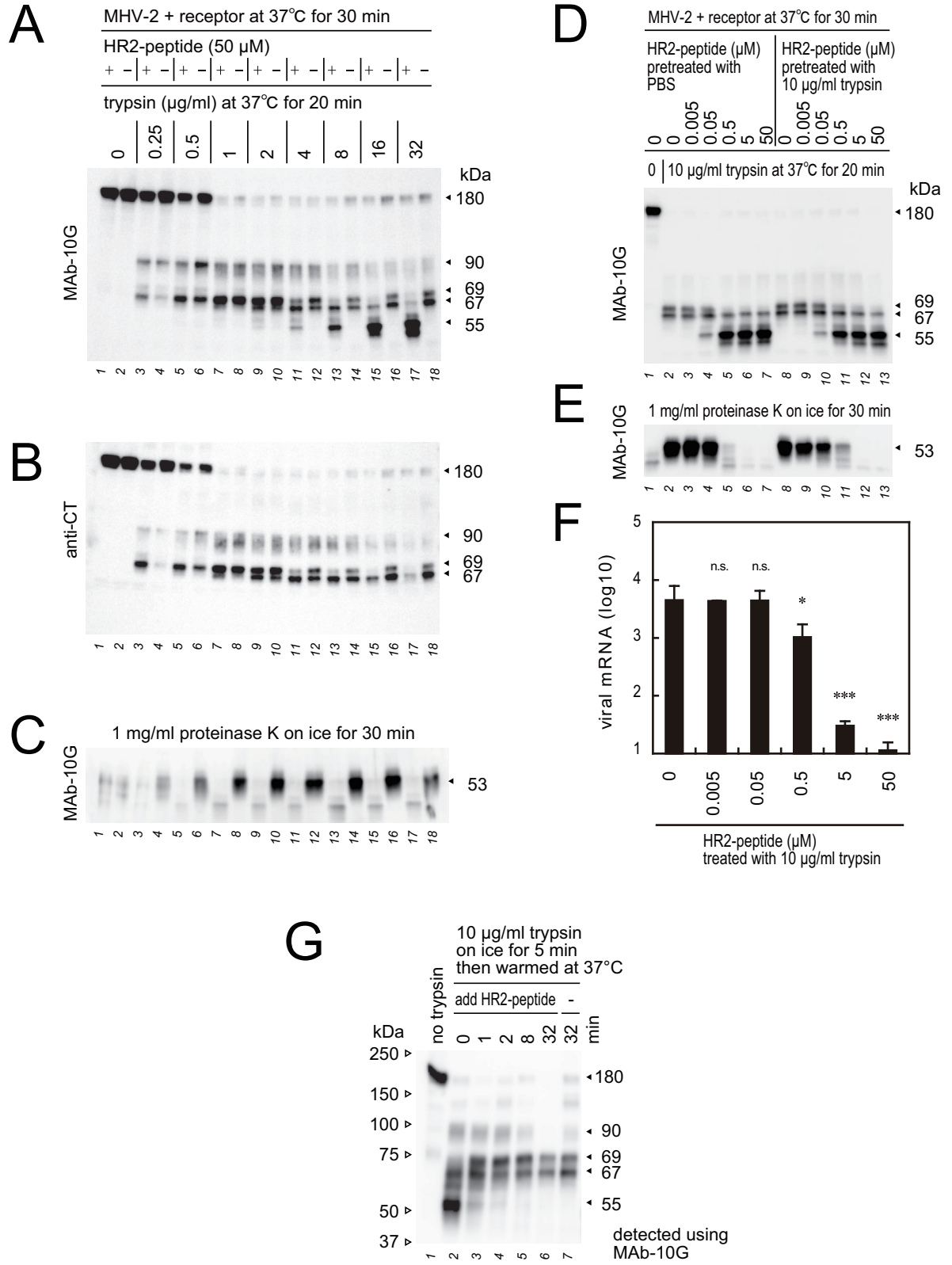


Fig. 9

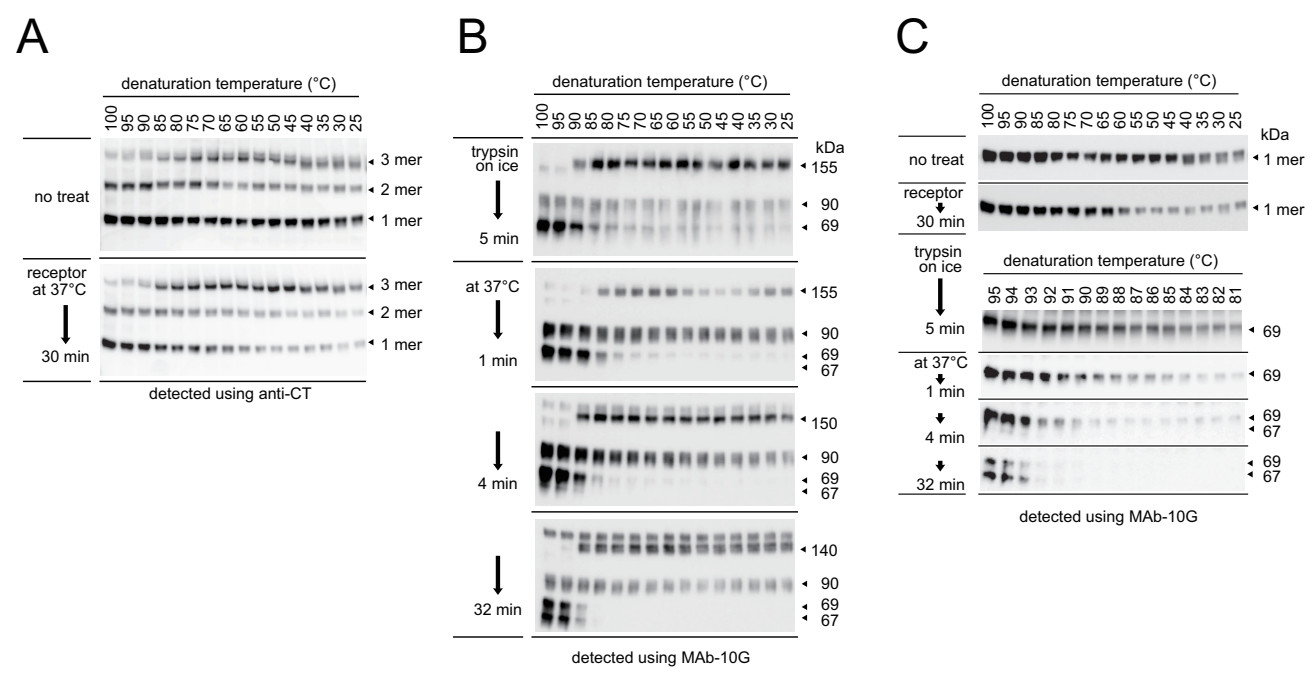


Fig. 10

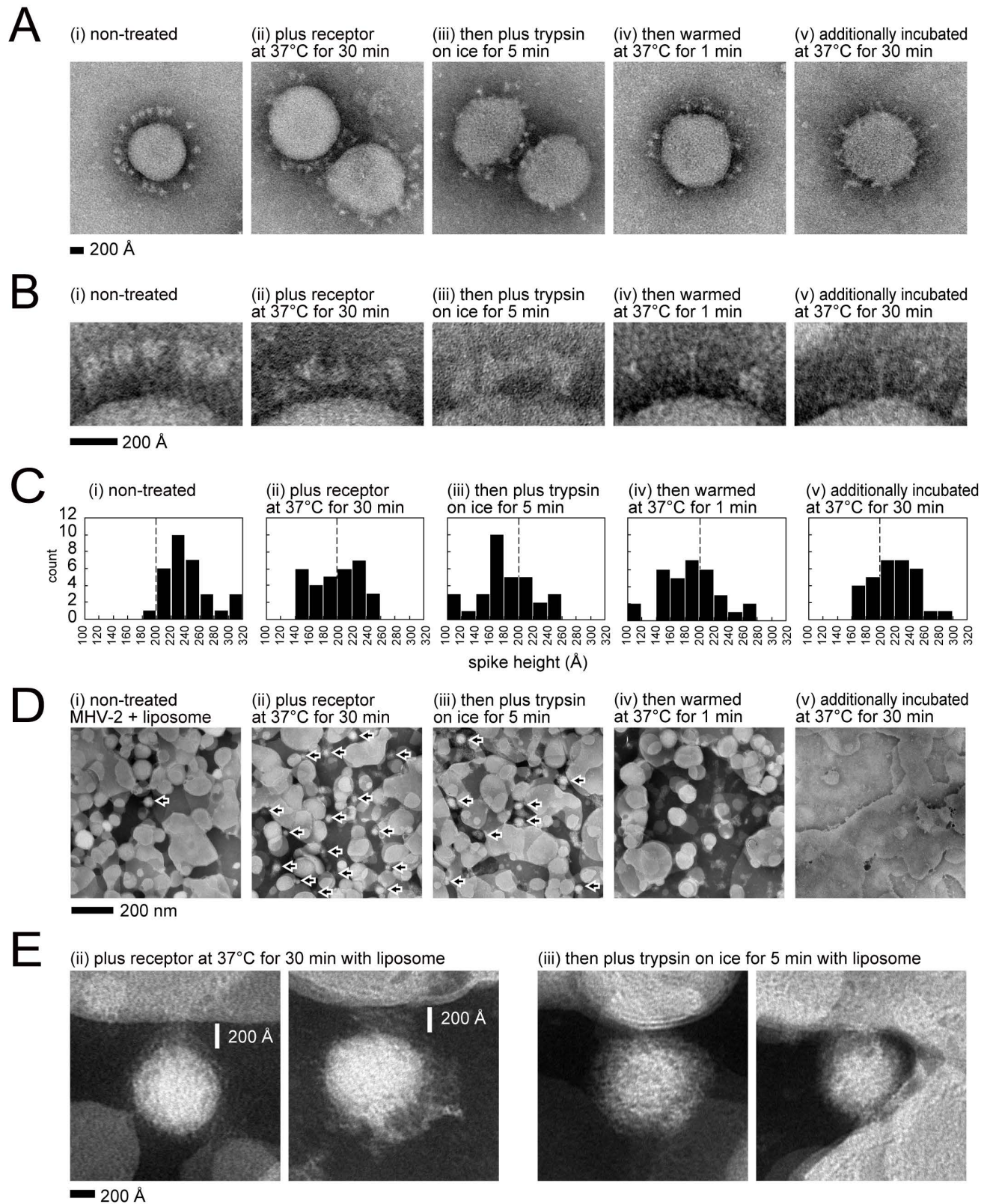


Fig. 11

